Molecular Therapy
Original Article

Ex vivo and *in vivo* suppression of SARS-CoV-2 with combinatorial AAV/RNAi expression vectors

Jonas Becker,[1,2,10] Megan Lynn Stanifer,[3,4,10] Sarah Rebecca Leist,[5,10] Bettina Stolp,[6] Olena Maiakovska,[1] Ande West,[5] Ellen Wiedtke,[1] Kathleen Börner,[1,7,8,12] Ali Ghanem,[1] Ina Ambiel,[5] Longping Victor Tse,[5] Oliver Till Fackler,[6,7] Ralph Steven Baric,[5] Steeve Boulant,[4,7,11] and Dirk Grimm[1,7,8,9,11]

[1]Department of Infectious Diseases/Virology, Medical Faculty, University of Heidelberg, BioQuant BQ0030, Im Neuenheimer Feld 267, 69120 Heidelberg, Germany; [2]Faculty of Biosciences, University of Heidelberg, 69120 Heidelberg, Germany; [3]Department of Infectious Diseases/Molecular Virology, Medical Faculty, Center for Integrative Infectious Diseases Research (CIID), University of Heidelberg, 69120 Heidelberg, Germany; [4]Department of Molecular Genetics and Microbiology, College of Medicine, University of Florida, Gainesville, FL 32611, USA; [5]Department of Epidemiology, University of North Carolina, 3304 Michael Hooker Research Building, Chapel Hill, NC 27599, USA; [6]Department of Infectious Diseases/Integrative Virology, Medical Faculty, Center for Integrative Infectious Diseases Research (CIID), University of Heidelberg, 69120 Heidelberg, Germany; [7]German Center for Infection Research (DZIF), Partner Site Heidelberg, 69120 Heidelberg, Germany; [8]Department of Infectious Diseases/Virology, Medical Faculty, Center for Integrative Infectious Diseases Research (CIID), University of Heidelberg, 69120 Heidelberg, Germany; [9]German Center for Cardiovascular Research (DZHK), Partner Site Heidelberg, 69120 Heidelberg, Germany

Despite rapid development and deployment of vaccines against severe acute respiratory syndrome coronavirus 2 (SARS-CoV-2), clinically relevant modalities to curb the pandemic by directly attacking the virus on a genetic level remain highly desirable and are urgently needed. Here we comprehensively illustrate the capacity of adeno-associated virus (AAV) vectors co-expressing a cocktail of three short hairpin RNAs (shRNAs; RNAi triggers) directed against the SARS-CoV-2 *RdRp* and *N* genes as versatile and effective antiviral agents. In cultured monkey cells and human gut organoids, our most potent vector, SAVIOR (SARS virus repressor), suppressed SARS-CoV-2 infection to background levels. Strikingly, in control experiments using single shRNAs, multiple SARS-CoV-2 escape mutants quickly emerged from infected cells within 24–48 h. Importantly, such adverse viral adaptation was fully prevented with the triple-shRNA AAV vector even during long-term cultivation. In addition, AAV-SAVIOR efficiently purged SARS-CoV-2 in a new model of chronically infected human intestinal cells. Finally, intranasal AAV-SAVIOR delivery using an AAV9 capsid moderately diminished viral loads and/or alleviated disease symptoms in hACE2-transgenic or wild-type mice infected with human or mouse SARS-CoV-2 strains, respectively. Our combinatorial and customizable AAV/RNAi vector complements ongoing global efforts to control the coronavirus disease 2019 (COVID-19) pandemic and holds great potential for clinical translation as an original and flexible preventive or therapeutic antiviral measure.

INTRODUCTION

With nearly 274 million infections worldwide of severe acute respiratory syndrome coronavirus 2 (SARS-CoV-2) and over 5.35 million deaths (as of December 21, 2021) related to the associated coronavirus disease 2019 (COVID-19) (https://www.who.int/publications/m/item/weekly-operational-update-on-covid-19—21-december-2021), the SARS-CoV-2 pandemic dramatically demonstrates the need for quickly customizable strategies to counteract emerging pathogens. So far, substantial hope and benefit is offered by an arsenal of vaccines that have been developed, clinically evaluated, and deployed at unprecedented speed.[1–4] Concurrently, numerous academic and industrial entities are investigating further modalities, including small molecules, repurposed drugs, oligonucleotide therapies, and monoclonal antibodies. Many compounds, such as hydroxychloroquine and ritonavir, failed to demonstrate clinical efficacy.[5] Remdesivir, the only small-molecule antiviral agent against SARS-CoV-2 currently approved by the US Food and Drug Administration and European Medicines Agency (EMA), moderately improves disease severity[6] and is currently not recommended by the World Health Organization (WHO) because of subpar efficacy in the SOLIDARITY trial.[7] Monoclonal antibodies seem to be more effective when given early, with three products approved via emergency use authorization by the FDA: monotherapy with bamlanivimab as well as combinations of bamlanivimab with etesevimab or casirivimab with imdevimab. All of these antibodies target the SARS-CoV-2 spike (S) glycoprotein[8,9] and were found to be capable of reducing viral loads.

The demand for additional antiviral strategies against SARS-CoV-2 remains very high for several reasons. One is the focus of most of the current vaccines and of all approved monoclonal antibodies on

Received 24 September 2021; accepted 12 January 2022;
https://doi.org/10.1016/j.ymthe.2022.01.024.

[10]These authors contributed equally

[11]These authors contributed equally

[12]Present address: AskBio GmbH, 69123 Heidelberg, Germany

Correspondence: Dirk Grimm, Department of Infectious Diseases/Virology, University of Heidelberg, BioQuant BQ0030, Im Neuenheimer Feld 267, 69120 Heidelberg, Germany.
E-mail: dirk.grimm@bioquant.uni-heidelberg.de

the S protein as an antigenic target. Hence, the dynamic occurrence of new variants of concern (VOCs) that are resistant and/or more infectious jeopardizes long-term effectiveness, as exemplified by the currently rapidly spreading omicron strain with 30 mutations in S. Additional concerns are sparked by mutation of viral strains that establish reservoirs in farmed animals.[10–16] Second, vaccine efficacy is dampened in immunocompromised or immunosuppressed subjects, leaving them susceptible to infection and vulnerable to the emergence of new variants of SARS-CoV-2.[17] Third, successful global protection from severe COVID-19 through vaccination critically relies on vaccine designs and formulations permitting storage, distribution and application at ambient temperature without the need for special cooling devices or uninterrupted cold chains.

Hence, it is key to explore alternative, adjunctive, or orthogonal antiviral strategies that are versatile enough to enable quick adaptation to emerging mutations, that do not rely on humoral or cellular immune responses, and whose physical properties and requirements are suitable for worldwide dissemination. An auspicious option is RNA interference (RNAi) induced by small interfering RNA (siRNA) or short hairpin RNA (shRNA), for which the RNA genomes and transcripts of CoVs, including SARS-CoV-2, pose an optimal target.[18] This has been experimentally validated for SARS-CoV *in vitro*[19] and *in vivo*[20] and is highly promising for SARS-CoV-2 as well, as exemplified recently. In one notable study, Idris et al.[21] harnessed intravenous injection of lipid nanoparticles to deliver chemically stabilized siRNAs against SARS-CoV-2 helicase or RNA-dependent RNA polymerase (RdRp) to murine lungs, resulting in mitigation of symptoms, including less weight loss, lower clinical score, and reduced viral titers in the lungs. However, the effect was transient and required multiple doses of the siRNA formulation.[21] Similarly, Gu et al.[22] reported an *in vivo* decrease in viral RNA copies in the lungs and tracheas of Syrian hamsters and rhesus macaques following repeated intranasal or intratracheal administration of anti-RdRp siRNA. Concurrently, many groups have published databases of computationally predicted RNAi targets in SARS-CoV-2 and matching siRNA sequences.[23–26] These RNAi approaches are complemented by exciting studies from multiple labs illustrating the power and potential of CRISPR-Cas13 systems to inhibit SARS-CoV-2 expression and replication on the RNA level *in vitro* and *in vivo*. These include Cas13a,[27] Cas13b,[28] and Cas13d[29] and comprise use of nebulizers for delivery of Cas13a mRNA and associated guides to lungs of mice and hamsters.[27]

Notwithstanding the promise of these approaches, a main limiting factor hampering their clinical translation is the need for tools for efficient, targeted, and safe delivery of RNAi or CRISPR compounds to the sites of infection. In this respect, the most promising options are vectors based on non-pathogenic adeno-associated viruses (AAVs), which have already been studied extensively as an antiviral modality.[30] In these, a single-stranded DNA of up to 5 kb is flanked by inverted terminal repeats (ITRs; AAV packaging elements) and encapsidated in a naked protein shell. A major benefit of AAVs is the ability to harness capsids derived from countless natural or synthetic viral variants in a process called pseudotyping,[31] enabling specific targeting of most tissue and cell types across species. Moreover, smaller cargos below 2.4 kb can be encapsidated as so-called self-complementary DNA (scDNA) that is flanked by one wild-type and one mutated ITR,[32] which enables faster transgene expression because self-complementary AAVs (scAAVs) immediately form transcriptionally active double-stranded DNA in the transduced cell. Together with the safe and persistent gene expression noted in over 200 clinical trials,[30] these features make AAV a superior vector for human gene therapy applications and led to FDA approval of the AAV drugs Luxturna and Zolgensma.[33]

Here we demonstrate the capacity of pseudotyped scAAV vectors co-expressing multiple shRNAs against conserved targets in SARS-CoV-2 nucleocapsid (*N*) and *RdRp* to inhibit viral replication and spread in a variety of *ex vivo* and *in vivo* model systems. Importantly, we provide experimental evidence for the high propensity of SARS-CoV-2 to escape suppression by a single RNA inhibitor through rapid mutation and document the ability to thwart this concern by multiplexing three independent shRNAs in a single AAV. Finally, we illustrate the potential of a selected vector, AAV-SARS virus repressor (SAVIOR), to mitigate disease symptoms and/or lower viral loads in two different mouse models of SARS-CoV-2 infection, highlighting the great promise of this direct-acting antiviral vector and its future permutations to complement current vaccine or therapy regimens for COVID-19.

RESULTS

Selection and validation of anti-SARS-CoV-2 shRNAs in cultured cells

Based on the genomic sequence of SARS-CoV-2 available in early 2020 (see Materials and methods for details), we initially selected 19 anti-SARS-CoV-2 shRNAs (Table S1) against the viral *RdRp* and *N* genes (Figure 1A; shRNAs C1–C19). We focused on these two targets because the polymerase governs viral genome replication, whereas the N protein is crucial for viral particle assembly and RNA genome packaging. In addition, three shRNAs (C20–C22) were directed against the human angiotensin-converting enzyme 2 (hACE2), the entry receptor for SARS-CoV-2.[34] We then harnessed Vero E6 cells, which are highly susceptible to SARS-CoV-2 infection and express hACE2,[35] to assess the efficacy of these 22 shRNAs. The shRNAs were expressed from a U6 RNA polymerase III promoter, encoded in scAAV vectors (one shRNA per vector) and packaged into the AAV-LK03 capsid,[36] which we had identified as a potent transducer in these cells (Figure S1). In this primary screen (Figure 1B), Vero E6 cells were pretreated with equal aliquots of cell lysates containing non-purified AAV-shRNA vectors. After 3 days, cells were infected with SARS-CoV-2, and infection was assayed 24 h later by immunostaining infected cells using an antibody against double-stranded RNA (dsRNA) (Figure 1C; infected cells containing dsRNA are shown in green, whereas the red color originates from non-specific staining of all cells per well with Draq5).

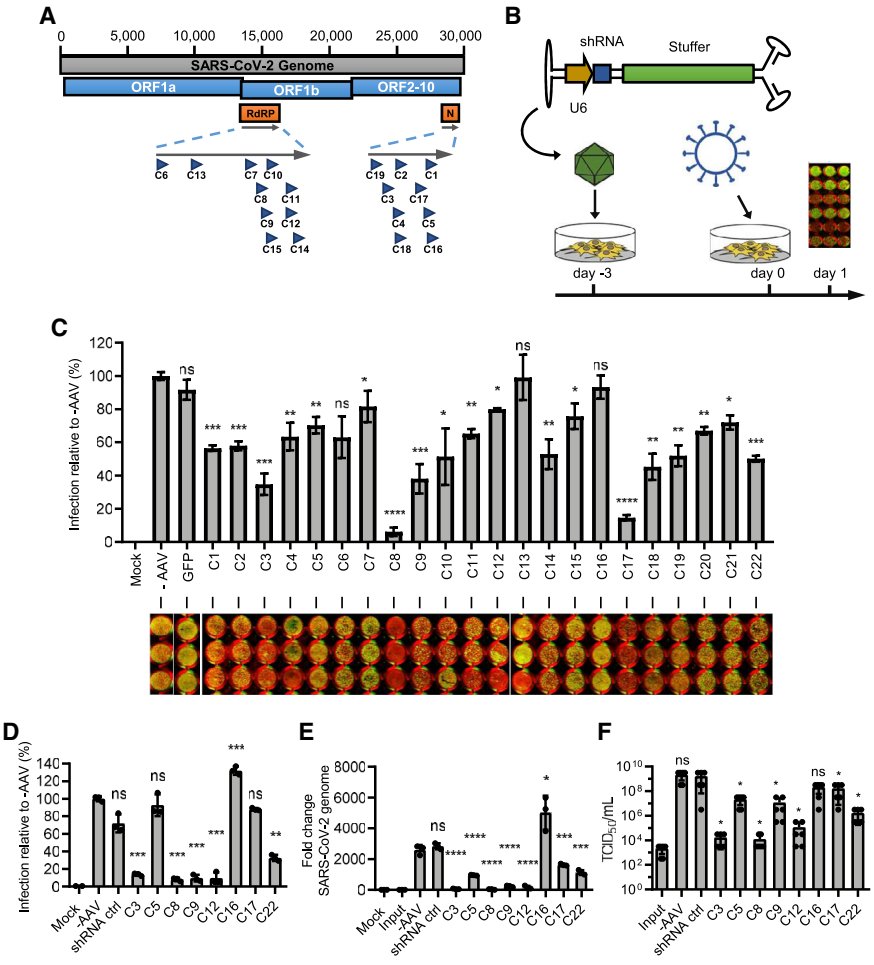

Figure 1. Identification of potent shRNAs against SARS-CoV-2 in Vero E6 cells

(A) Binding sites of shRNAs C1-C19 in the *RdRp* and *N* genes of SARS-CoV-2. (B) Schematic of scAAV vectors used for screening of potent shRNA candidates in Vero E6 cells by transduction on day −3 (MOI of 10^5), followed by infection with SARS-CoV-2 (MOI of 3) on day 0 and quantification of SARS-CoV-2 infection by indirect IF assay using an antibody against double-stranded RNA (dsRNA) on day 1 (n = 3 wells per condition). (C) Fluorescent antibody-mediated detection of dsRNA as a surrogate for SARS-CoV-2 infection in Vero E6 cells, following transduction with AAV vectors encoding shRNAs C1–C22. Ctrls were non-transduced (−AAV) or mock-infected cells or cells transduced with a GFP-encoding vector. Original images at the bottom show cell nuclei in red (Draq5) and infected cells (anti-dsRNA antibody) in green. Non-transduced cells were used for normalization of SARS-CoV-2 infection in each sample. (D–F) Validation of promising candidates via measurement of (D) relative fluorescence after dsRNA antibody staining normalized to non-transduced cells, (E) fold change of SARS-CoV-2 genome copy numbers by qPCR compared with input, and (F) titers of infectious virus by $TCID_{50}$ assay. Data are means ± SD. ns, non-significant; *p ≤ 0.05; **p ≤ 0.01; ***p ≤ 0.001; ****p ≤ 0.0001.

The capacity of each individual shRNA to interfere with SARS-CoV-2 infection was addressed by measuring the relative fluorescence intensity of the infected samples and by normalizing it to mock-infected cells (Figure 1C top). This identified several promising candidates, a subset of which we subsequently validated in secondary screens using purified and titrated AAV vectors. Therefore, Vero E6 cells were pretreated with equal amounts of selected AAV-shRNA vectors, and 3 days later, cells were infected with SARS-CoV-2. After another 24 h, SARS-CoV-2 infection, replication, and production of new infectious virus particles were assessed by immunostaining against dsRNA (Figure 1D), quantitative reverse transcriptase PCR (Figure 1E) and $TCID_{50}$ titration (Figure 1F), respectively. The shRNAs C3 (targeting *N*) and C8 and C12 (both targeting *RdRp*) were most efficient in interfering with SARS-CoV-2 infection, as determined by the reduction of the number of infected cells (Figure 1D), of SARS-CoV-2 genome replication (Figure 1E), and of the amount of infectious virus particles released by infected cells (Figure 1F).

Two of the eight shRNAs in the secondary screen, C12 and C17, behaved differently from the primary screen (Figures 1C and 1D). This can be attributed to the use of non-purified and non-titrated crude cell lysates in the first screen and the ensuing inherent uncertainties regarding vector doses in such "quick and dirty" screens, as we and others have observed before.[37,38] Accordingly, the results of the secondary validation screen, which were consistent with the primary screen for the other six shRNAs, are more reliable and were used as the basis for all subsequent work.

These results illustrate the capacity of scAAV vectors encoding shRNAs directed against SARS-CoV-2 (C1–C19) to significantly interfere with viral infection in susceptible cells. The three vectors C20–C22, expressing anti-hACE2 shRNAs, also suppressed SARS-CoV-2 infection (Figures 1D and 1F), consistent with the role of hACE2 as a SARS-CoV-2 entry receptor and concurrent with the ability of these shRNAs to inhibit ACE2 expression in Vero E6 cells (Figure S2).

Multiplexing of the best shRNAs in the AAV-SAVIOR vector

Previously, we and others had proposed and validated the concept of combinatorial RNAi; i.e., concurrent delivery of multiple siRNAs or shRNAs to the same cell to boost knockdown efficiency or, in the case of viral targets, to counteract escape by mutation.[39–42] To study whether this concept would also prove beneficial in the context of SARS-CoV-2 infection, we multiplexed the three most potent shRNAs in a single AAV genome using our TRISPR platform,[43] a scAAV backbone permitting co-expression of three different shRNAs

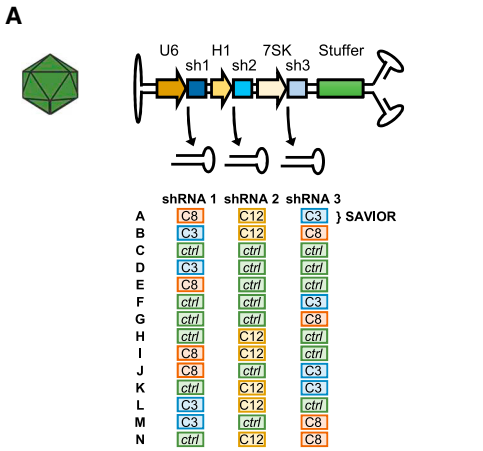

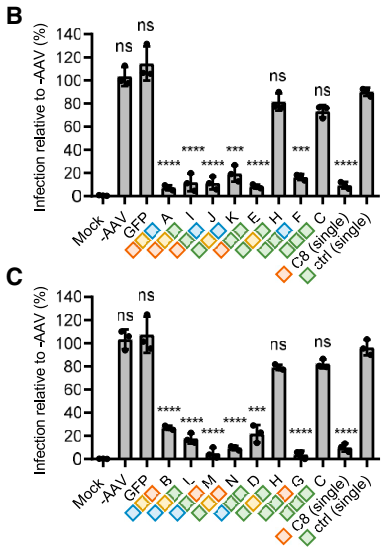

Figure 2. Multiplexing of shRNA lead candidates in the AAV-TRISPR format

(A) Configurations of AAV-TRISPR vectors containing three expression cassettes in which the U6, H1, and 7SK promoters drive expression of the anti-SARS-CoV-2 shRNAs C3, C8, and C12 in various permutations, including a non-targeting control (ctrl) shRNA. (B and C) Quantification of SARS-CoV-2 infection of Vero E6 cells with the indirect IF assay normalized to non-transduced cells (−AAV; set to 100%). Cells were pretreated with vector lineages derived from (B) TRISPR-A (shRNA C8 in position 1 under the U6 promoter) or (C) TRISPR-B (shRNA C3 in position 1 under the U6 promoter) (n = 3 wells per condition). Data are means ± SD. ns, non-significant; ***p ≤ 0.001; ****p ≤ 0.0001.

under the RNA polymerase III promoters U6, H1, or 7SK, respectively (Figure 2A). For the two vectors TRISPR-A (U6-C8:H1-C12:7SK-C3) and TRISPR-B (U6-C3:H1-C12:7SK-C8), we also created permutations carrying a control (ctrl) shRNA at each position (TRISPR-C to -N), including the triple-ctrl construct TRISPR-C. Analysis in the Vero E6 infection assay showed that TRISPR-A (hereafter called SAVIOR) was able to interfere with SARS-CoV-2 infection in a manner comparable with the most robust single-shRNA vector (TRISPR-E, only expressing C8) and outperformed TRISPR-B as well as most other constructs and ctrls (Figures 2B and 2C). This was confirmed in luciferase reporter assays (Figure S3), where the two TRISPR variants encoding all three shRNAs (TRISPR-A and -B) were superior to most other constructs containing only one or two shRNAs. The fact that the relative knockdown efficiencies differed slightly between the infection (Figure 2) and reporter (Figure S3) assays can likely be explained by the inherent differences in the targets and readouts, including use of a replication-competent virus (Figure 2). Importantly, both assays consistently verify that each of the three shRNAs is functional, as evidenced by the SARS-CoV-2 (Figure 2) and luciferase (Figure S3) knockdown obtained with TRISPR-E (C8 shRNA only), TRISPR-F (C3 shRNA only), and TRISPR-H (C12 shRNA only).

We also analyzed the integrity of the AAV vector constructs carrying multiple shRNA expression cassettes, based on data showing that secondary shRNA structures can act as cryptic ITRs and trigger packaging of truncated genomes.[44] Although the latter was indeed observed (Figure S4), we detected ∼65% full-length genomes in TRISPR-A or -C vector stocks, which we consider reasonable. Still, future optimization of downstream manufacturing should aim to eliminate the ∼35% of byproducts.

As noted, our rationale for creating a triple-shRNA vector included the concern that SARS-CoV-2 knockdown using single shRNAs may create selection pressure, forcing the evolution of escape mutants that acquired resistance to the respective shRNA. This concern has also been raised previously in the context of siRNA- or CRISPR-Cas13-based anti-SARS-CoV-2 strategies,[21,27,28] but, to the best of our knowledge, has never been experimentally validated. Hence, we expected that simultaneous targeting of three independent sites in the SARS-CoV-2 genome should prevent viral escape. For experimental verification, we passaged SARS-CoV-2 in Vero E6 cells that were pre-transduced with a single shRNA vector (encoding C3, C8, C12, or ctrl shRNAs) or the multiplexed SAVIOR or TRISPR-C vectors (Figure 3A). As predicted, daily virus passaging over a period of eight passages in the presence of the single C3 and C12 vectors consistently triggered rapid viral breakthrough already after one to three passages (Figures 3B and 3C). Even with the most robust single C8 vector, virus rebound was observed in one of the three biological replicates. In striking contrast, the multiplexed SAVIOR construct yielded efficient knockdown over all eight passages without evidence of viral breakthrough, supporting the predicted benefit of the triple-shRNA design.

Sanger sequencing of the single-shRNA samples confirmed the emergence of point mutations in the respective shRNA binding sites (Table S2; Figure 4A). To experimentally confirm that these mutations lower the susceptibility to shRNA knockdown, we created luciferase reporters containing all permutations of the three wild-type or mutated binding sites in their 3′ UTRs (Figure S5A). When co-transfected with the individual shRNA plasmids or TRISPR-A, we typically measured a reduced knockdown efficiency of the mutated binding sites with the cognate single shRNA compared with the genuine binding site (Figure S5B). In all cases, TRISPR-A very potently suppressed the luciferase reporters tagged with any combination of one or two mutated binding sites. A marginal reduction in TRISPR-A knockdown efficiency was only observed for the reporter in which all three binding sites were mutated concurrently, but even in this case, the triple-shRNA construct clearly outperformed all individual shRNA plasmids (Figure S5B).

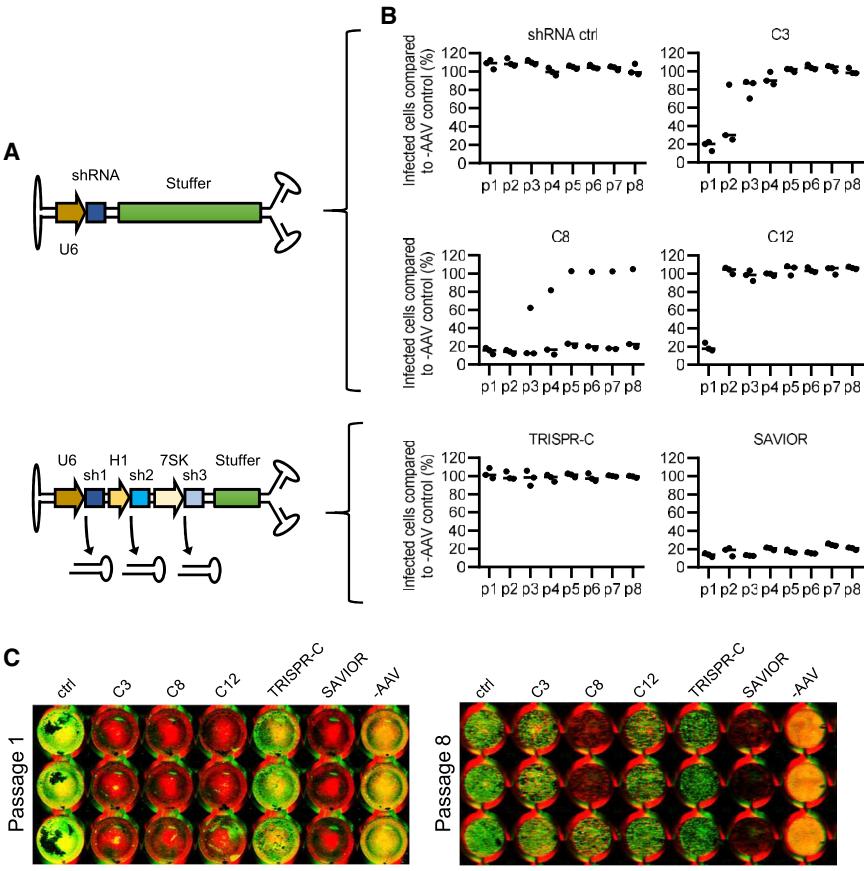

Figure 3. Prevention of viral breakthrough with AAV-SAVIOR

(A) Schematic of all vectors used in this experiment. (B) Results from passaging of SARS-CoV-2 every 24 h on Vero E6 cells transduced with single shRNA vectors (shRNA ctrl, C3, C8, or C12) or with AAV-SAVIOR or the corresponding TRISPR-C ctrl vector. Percentages of infected cells were measured for each passage and normalized to infected but non-transduced (−AAV) cells. (C) Representative original images of the indirect IF assay used to calculate the data in (B).

To investigate whether the nucleotide variations detected in the escaped SARS-CoV-2 replicates were found in published SARS-CoV-2 genome sequences as well, we aligned 365,255 full-length SARS-CoV-2 genomes and performed single-nucleotide variant (SNV) calling for the C3, C8, and C12 shRNA binding sites (Figure 4B, Table S3). Among the aligned sequences, the A > T mutation we found after passaging with the C8 shRNA (position 15,312) was detected 8 times, the C > T mutation in C12 (pos. 15,848) 358 times, and the C > T in C3 (pos. 28,486) 103 times. The T > C mutation in C3 (pos. 28,489) was not detected. This implies that these escape variants had primarily evolved because of the selective pressure of each individual shRNA. Although six GenBank sequences were found to have variant nucleotides in two of the three shRNA target sites (C8 and C12; reference numbers OA997044.1, MZ159230.1, MW550403.1, MZ153737.1, OD908225.1, and MZ398586.1), none had mutations in all three sites targeted by the SAVIOR construct.

Therefore, our results confirm the aforementioned general concern that RNAi-based antiviral strategies can lead to selection of escape mutants that have developed resistance against a single RNAi trigger. Most importantly, our data show that targeting multiple sites in SARS-CoV-2 with different shRNAs from a combinatorial AAV vector prevents the generation or outgrowth of such viral escape mutants, highlighting the translational potential of AAV-SAVIOR.

An alignment of 40,000 randomly selected, full-length SARS-CoV-2 genomes illustrates that the three shRNA target sites of SAVIOR do not lie within regions of major variability (Figure 4C). Here we performed this analysis retrospectively, based on shRNAs that we had already selected at the beginning of the pandemic, when fewer SARS-CoV-2 strains were known. In the future, as demonstrated by others,[23–26] such an analysis can ideally be used to proactively identify optimal shRNA target regions with maximum conservation across SARS-CoV-2 variants, facilitating development of broadly active, next-generation AAV-SAVIOR permutations.

Validation of AAV-SAVIOR in chronically infected cells and human gut organoids

Next we wanted to determine whether AAV-shRNA-mediated knockdown could also provide a curative benefit for cells that are already infected with SARS-CoV-2. When infecting the human colon carcinoma-derived cell line Caco-2 with SARS-CoV-2 at a high multiplicity of infection, we noticed that most of the cells died within the first 48 h of infection, whereas about 10% of them continued growing and dividing. Interestingly, we found that these cells were also infected by SARS-CoV-2 and could be passaged as a chronically infected cell clone that supported SARS-CoV-2 replication and secretion of *de novo* infectious virus particles (data not shown). Transduction of these chronically infected human intestinal Caco-2 cells with SAVIOR largely reduced virus replication in cells, as monitored by quantitative reverse transcriptase PCR against the SARS-CoV-2 genome (Figure 5A), and the number of infectious particles released by the cells (Figure 5B). Five days after transduction with SAVIOR, SARS-CoV-2 replication was reduced to undetectable levels (Figure 5A), and only little amounts of *de novo* infectious virus particles were

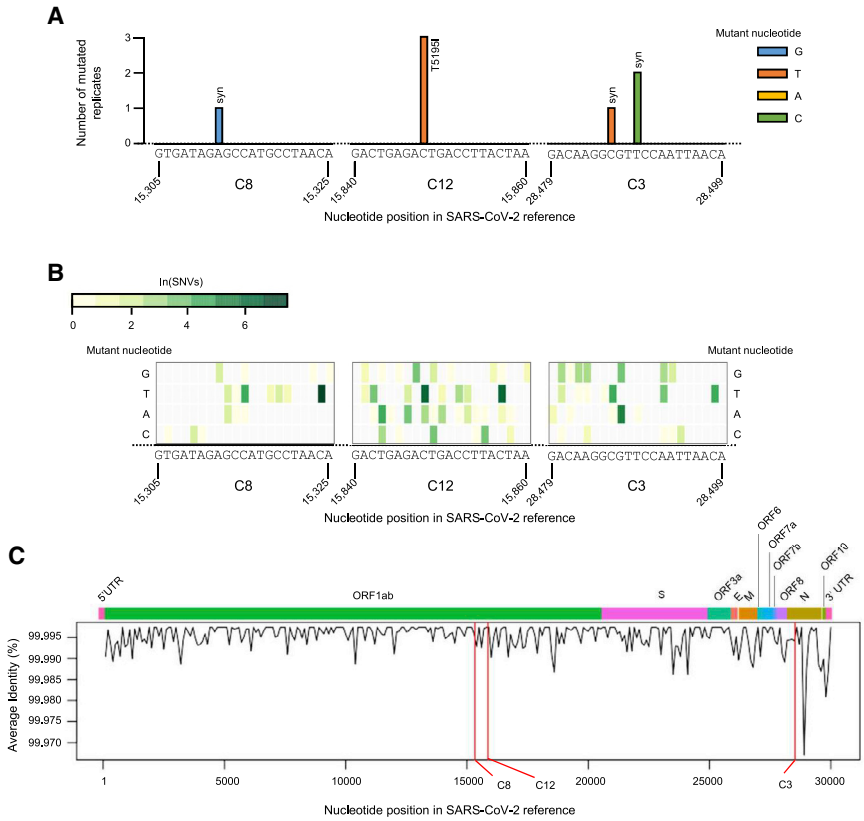

Figure 4. Bioinformatics analysis of shRNA target site conservation in SARS-CoV-2 strains

(A) Mutations detected in SARS-CoV-2 shRNA binding sites after passaging in AAV-pretreated Vero E6 cells and numbers of respective occurrences within the triplicate measurement (Figure 3 and Table S2). Mutant sequences were determined by Sanger sequencing of PCR amplicons within *RdRp* and *N* genes obtained by PCR amplification of reverse-transcribed RNA from the cell supernatants. (B) Natural logarithm of numbers of SNV occurrences within C3, C8, and C12 shRNA binding sites revealed from variant-calling analysis of 365,255 full-length SARS-CoV-2 genomes. (C) Average identity (percent) of 40,000 randomly selected, full-length SARS-CoV-2 genomes with positions of C8, C12, and C3 binding sites in *ORF1ab* (C8 and C12) or *N* (C3), respectively.

released by the originally chronically infected cells (Figure 5B). In the $TCID_{50}$ assay measuring SARS-CoV-2 progeny, the triple-shRNA vector outperformed the best single-shRNA vector encoding the C8 shRNA at all time points (Figure 5B).

To determine whether SAVIOR can actively interfere with SARS-CoV-2 infection in non-transformed human cells, we used primary human ileum and colon epithelial cells, which are physiologically relevant targets for SARS-CoV-2 infection.[45,46] These cells were grown as mini-gut organoids and fully supported SARS-CoV-2 infection, replication, and spread.[47] Pre-treatment of these mini-gut organoids with SAVIOR or the single-shRNA C8 vector resulted in almost complete prevention of SARS-CoV-2 infection of primary human intestinal epithelial cells (Figure 6A and 6B).

Our data demonstrate that AAV-SAVIOR does not solely act in a prophylactic manner but can also be used after cell infection and actively cure infected cells.

In vivo modulation of SARS-CoV-2 replication and pathogenesis in two different mouse models of infection

To evaluate our vectors' ability to act as a prophylactic agent that mitigates wild-type SARS-CoV-2 infection and associated symptoms *in vivo*, we harnessed an established mouse model, K18-hACE-2 transgenic mice (Figure 7A). These mice were inoculated intranasally with 2×10^{11} vector genomes (vg) of AAV-SAVIOR or the TRISPR-C ctrl vector packaged into the AAV9 capsid before infection with 5×10^4 plaque-forming units (PFUs) of wild-type SARS-CoV-2 7 days later (n = 4 mice per group). As additional ctrls, wild-type littermates were treated identically. Body weight and disease score were monitored daily until the transgenic mice reached the maximum disease score (Table S4) and qualified for euthanasia on day 5 or 6 after infection. Lung and brain tissues were collected, and from these, viral genomes and infectious titer (PFUs) of SARS-CoV-2 were determined.

As expected, wild-type mice did not show any symptoms upon infection with SARS-CoV-2, whereas hACE2-transgenic mice exhibited a decrease in body weight (Figure 7B) and an increasing disease score (Figure 7C and Table S4), with similar values for mice treated with SAVIOR and the TRISPR-C ctrl vector. Importantly, at the time of euthanasia, we measured a notable but not statistically significant trend toward a reduction of SARS-CoV-2 genome copy numbers (17.4-fold) and infectious units (2.9-fold) in the lungs of hACE2-transgenic mice treated with AAV-SAVIOR compared with the TRISPR-C ctrl (Figures 7D and 7F). Compared with the lungs, SARS-CoV-2 copy numbers and infectious units were markedly higher in the brains of all infected animals and unaffected by treatment with AAV-SAVIOR, as expected from intranasal vector delivery (Figures 7E and 7G). Massive infection of the brain is a well-known characteristic feature of this particular animal model and a major cause of morbidity upon SARS-CoV-2 infection.[48] Infection rates in the lungs and brains of wild-type ctrl mice lacking hACE2 were below the detection limit of both assays, in line with the aforementioned lack of symptoms in these animals.

We subsequently evaluated AAV-SAVIOR more extensively in a second murine challenge model using wild-type BALB/c mice and

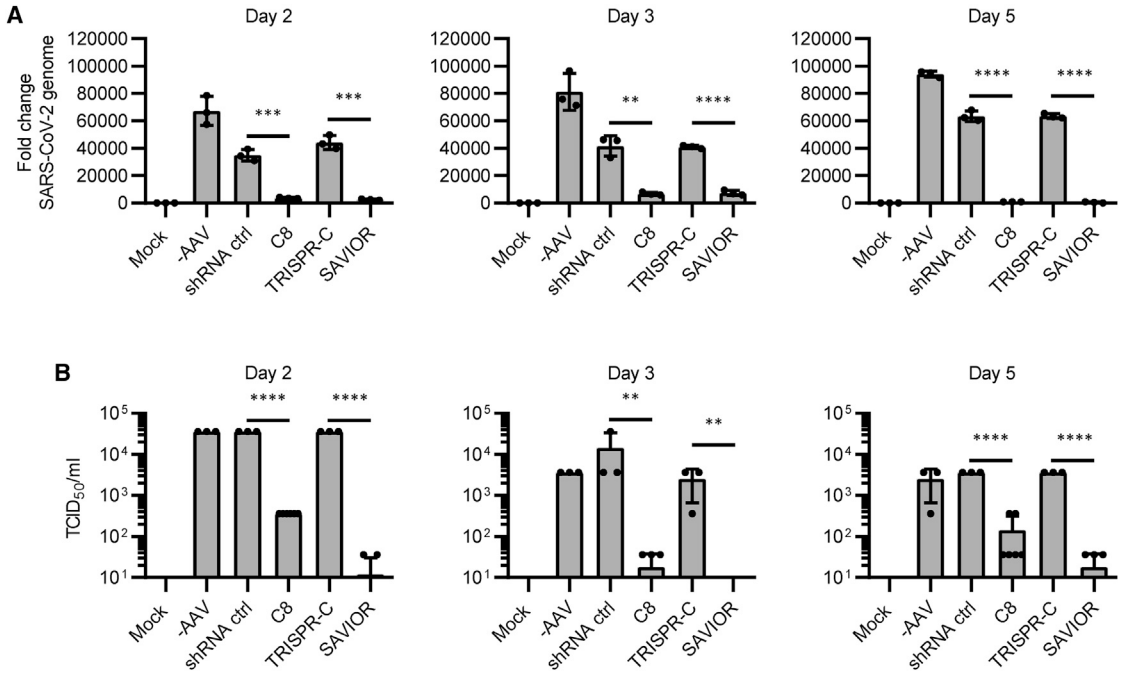

Figure 5. SARS-CoV-2 suppression with AAV-SAVIOR in chronically infected Caco-2 cells

(A and B) Transduction of Caco-2 cells chronically infected with SARS-CoV-2 with single shRNA vectors encoding C8 or ctrl shRNA or with AAV-SAVIOR or the corresponding TRISPR-C ctrl. Additional ctrls were mock-infected or non-transduced (−AAV) Caco-2 cells. (A) Fold change of SARS-CoV-2 genome copy numbers relative to virus input, as measured by qPCR 2, 3, or 5 dpi. (B) Quantification of infectious SARS-CoV-2 particles 2, 3, or 5 dpi by $TCID_{50}$ assay (n = 3 wells per condition). Data are means ± SD. **$p \leq 0.01$; ***$p \leq 0.001$; ****$p \leq 0.0001$.

the mouse-adapted SARS-CoV-2-MA10 strain, which accurately reflects the lung disease phenotype seen in humans (Figure 8A).[49] Focusing on this alternative model based on a wild-type, immunocompetent strain provided several benefits, especially the fact that we could more easily upscale animal numbers as well as study and compare young and old mice, with the latter best reflecting human disease progression and sequelae. Moreover, we used a 5-fold lower dose of SARS-CoV-2 in these experiments, which sufficed to establish robust infection and may concurrently better approximate the conditions of natural transmission among humans. Finally, unlike the K18-hACE2-transgenic model used above, the MA10 model is not restricted by excessive SARS-CoV-2 infection of the brains of the animals and the morbidity and mortality associated with this neuroinvasion.

Specifically, 10-week-old ("young") or 1-year-old ("old") BALB/c mice were transduced intranasally with 2×10^{11} vg per mouse of AAV-SAVIOR (the same dose as used before in the K18-hACE-2 model), TRISPR-C, or a second ctrl encoding enhanced GFP (EGFP), all packaged in AAV9 (n = 5 mice per group). One or two weeks later, the animals were challenged with 1×10^4 PFUs of SARS-CoV-2-MA10. Body weight and airway resistance were monitored daily, and lungs were harvested 2 or 4 days post infection (dpi) for physiological, pathological, and viral load analyses (Figure 8A).

First, similar to the K18 model, we pre-treated young mice with AAV-SAVIOR, followed 1 week later by SARS-CoV-2-MA10 infection. This yielded multiple lines of clear evidence of a protective effect of our vectors, including the finding that treated mice were resistant to body weight loss after challenge, a hallmark of protection in the pathogenic SARS-CoV-2-MA10 model (Figure 8B). Furthermore, physiological indicators in AAV-SAVIOR-treated mice, including airway obstruction and lung hemorrhage, showed non-significant improvements compared with the ctrls. These trends include a reduction of PenH and EF50 scores in SAVIOR-treated mice on days 2 and 3 as well as a positive effect on hemorrhage scores (HSs). Although not reaching statistical significance in the overall cohort, viral lung titers of individual mice treated with AAV-SAVIOR were strongly reduced by up to 100-fold at 2 dpi (the peak titer of the MA10 model) (Figure 8B). At 4 dpi, we still observed a minor but noticeable trend toward a reduction in lung titer (Figure 8B).

To study the longevity of AAV-SAVIOR-mediated protection against SARS-CoV-2 infection, we next treated the mice 2 weeks before challenge, which is outside of the therapeutic windows of the current biologic treatments, including neutralizing antibodies (nAbs), antiviral peptides, and small-molecule drugs. Under these conditions, we observed no protective effect of AAV-SAVIOR compared with the two ctrls in terms of body weight loss or airway congestion scores (Figure S6). HSs showed a significant reduction

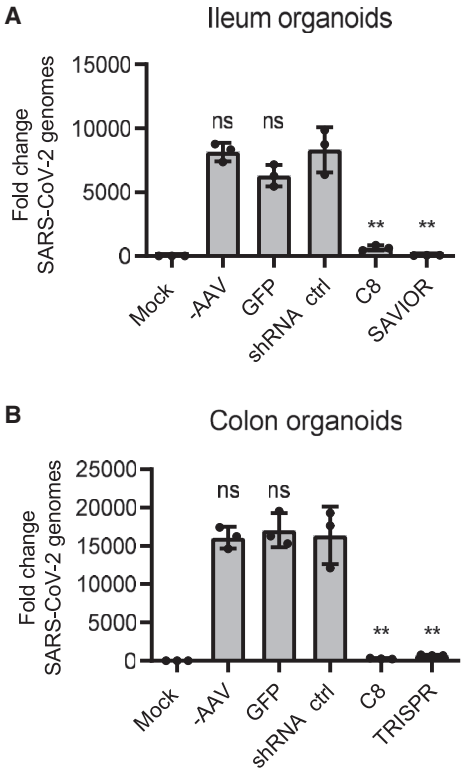

Figure 6. SARS-CoV-2 suppression with AAV-SAVIOR in human gut organoids

(A and B) Infection of primary human gut organoids with SARS-CoV-2 after transduction with single shRNA vectors encoding C8 or ctrl shRNA or with AAV-SAVIOR or the corresponding TRISPR-C ctrl. Additional ctrls were mock-infected or non-transduced (−AAV) organoids. (A) Fold change of SARS-CoV-2 genome copy numbers in human ileum organoids. (B) Fold change of SARS-CoV-2 genome copy numbers in human colon organoids (n = 3 wells per condition). Data are means ± SD. ns, non-significant; **$p \leq 0.01$.

compared with the TRISPR-C but not the EGFP ctrl. Although there was no difference in lung viral titers at 2 dpi, a non-statistically significant reduction was observed at 4 dpi. Specifically, two of five mice showed a 10- and 100-fold reduction in viral lung titer, respectively, suggesting rapid viral clearance (Figure S6).

To also assess the potential of AAV-SAVIOR in human populations that are less capable of mounting robust immune responses following traditional vaccination, we used an aged mouse model (1 year old) that better reflects the physiology and disease progression of severe infection in humans. When administered 1 week before SARS-CoV-2-MA10 challenge, AAV-SAVIOR treatment reduced body weight loss compared with ctrl treatments (Figure 8C). AAV-SAVIOR-treated mice also showed non-significant improvements in physiological markers, including lung HSs and airway congestion scores 2 dpi (HS and PenH) (Figure 8C). This therapeutically relevant benefit was consistent with a significant reduction in lung viral titers in AAV-SAVIOR-treated mice compared with both ctrls. The fact that this effect was noted at 4 but not at 2 dpi (Figure 8C), the opposite of the results in young mice (Figure 8B), suggests kinetic differences of AAV-SAVIOR in young versus old animals that warrant further investigation.

To study whether shRNA multiplexing in AAV-SAVIOR could also prevent the rise of SARS-CoV-2 escape variants *in vivo*, we sequenced the regions of the viral genome targeted by the three shRNAs (C3, C8, and C12) in this vector. This revealed the absence of any mutations in the treatment or ctrl groups (data not shown) and thus implies an ability of AAV-SAVIOR to prevent spontaneous or shRNA-induced viral escape *in vivo*, congruent with and extending our cell culture data (Figure 4). Additional work including more ctrls is required to also verify this conclusion at later time points, which will be relevant for chronic SARS-CoV-2 infection in humans.

DISCUSSION

The outbreak of SARS-CoV-2 and its rapid escalation to a pandemic with over 270 million global infections not only drastically illustrates the threat posed to humans by members of the Coronaviridae family, but it also highlights our deficits in understanding, preventing, and counteracting viral zoonosis and spread. Fortunately, a powerful arsenal of newly emerging technologies has been established over the past decade in other contexts that can now be repurposed at unparalleled speed. Particularly notable is vaccination technology based on synthetic and formulated mRNA, which is already widely applied and which promises to slow or even halt the pandemic in combination with other measures. It is also becoming increasingly clear that the ultimate goal of herd immunity may be difficult to reach for numerous reasons, including the inherent propensity of SARS-CoV-2 to swiftly gain fitness and escape humoral immunity via mutation, as drastically illustrated by the currently circulating and rapidly disseminating omicon strain. Other confounding factors are that a considerable percentage of the human population opposes vaccination; that specific recipients, such as lactating women or ailing individuals, may have to be excluded from vaccination; and that the latter may fail because of a suppressed or compromised immune system or for other unknown reasons. Last but not least, currently accumulating evidence implies that vaccine immunity wanes at different rates in the nose and deep lungs; hence, even multiply vaccinated individuals may again eventually become susceptible to infection and virus transmission, further restricting chances of achieving herd immunity.

These facts and concerns raise an urgent need to develop and preclinically validate complementing, direct-acting antiviral strategies that promise full and long-lasting protection and/or cure from SARS-CoV-2 infection while overcoming the limitations of active vaccination approaches and their restriction to a subset of the human population. As implied by the sum of *ex vivo* and *in vivo* data reported here, the combinatorial AAV-SAVIOR vector may help to fill in this gap and complement other ongoing global efforts to curb the pandemic, based on a variety of clinically pertinent benefits, including efficacy, versatility, and translatability.

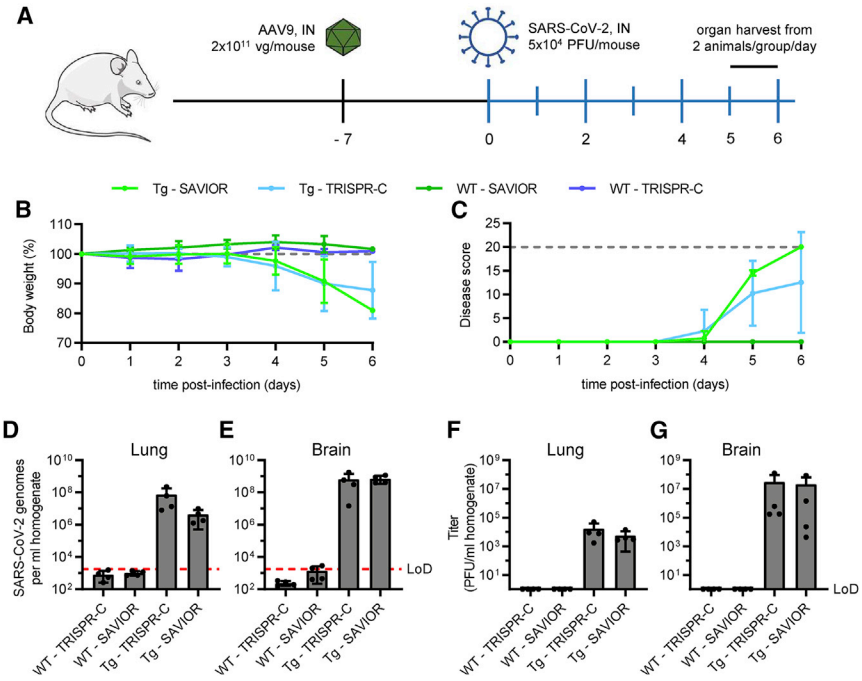

Figure 7. Use of AAV-SAVIOR for wild-type SARS-CoV-2 suppression in the lungs of hACE2-transgenic mice *in vivo*

(A) Experimental setup. K18-hACE2 transgenic (Tg) or wild-type (WT) mice were transduced intranasally with 2×10^{11} vg of AAV9 vectors 7 days prior to intranasal infection with 5×10^4 PFUs SARS-CoV-2 on day 0. Body weight and symptoms were monitored daily according to the score sheet in Table S4 until the maximum score was reached and animals were euthanized (n = 4 animals per group). (B) Body weight relative to day 0 after infection. The dashed gray line indicates initial body weight (100%). (C) Disease score according to the score sheet. The dashed gray line indicates the score where animals became eligible for euthanasia. Shown are mean values ±SD from four (0–5 days post infection [dpi]; two mice were harvested on day 5) or two (6 dpi) mice per time point. (D and F) Lungs and (E and G) brains were harvested and analyzed for viral load by qPCR for the SARS-CoV-2 *N1* gene (D and E) and for infectious viral titer by plaque assay on Vero E6 cells (F and G). The dashed red line indicates the limit of detection (LoD) of the assays, which is 1,810 genome copies per mL for the *N1* gene qPCR and 0 plaques/mL for the plaque assay. Each symbol represents an individual animal.

A first important finding in this work was that several of our initially tested shRNAs mediated robust inhibition of SARS-CoV-2 in cultured and infected cell lines or primary cells, akin to the results of colleagues who have successfully screened panels of siRNAs or CRISPR-Cas13a/b/d gRNAs before.[21,27–29] Further in line with data published in heterologous systems, we were not surprised to note that our best vector, AAV-SAVIOR, yielded knockdown efficiencies that were mostly similar to the single vector encoding our lead shRNA, C8. Identical findings were reported, for instance, by Fareh et al.,[28] who found no differences between an *N*-targeted crRNA pool versus their best individual crRNA, or by Idris et al.,[21] who observed that combining their three most potent siRNAs yielded the same SARS-CoV-2 knockdown efficiency as single siRNAs.

In all of these cases, including our own data, it is essential to note that multiplexing of RNAi or CRISPR triggers primarily aims to attack the virus at multiple sites, hampering its ability to escape by mutation, rather than to improve overall efficiency. The propensity of pathogenic viruses to rapidly develop resistance to a single inhibitor is a well-known and major concern regarding antiviral RNAi and CRISPR strategies, especially for RNA viruses with error-prone replication, such as HIV, hepatitis C virus (HCV), or poliovirus.[40,42,50–52] We considered it crucial to provide experimental evidence in this work that SARS-CoV-2 can indeed rapidly mutate and escape from a single shRNA because this concern has been raised multiple times before but, to our best knowledge, has never been verified to date. Strikingly, we found that the virus quickly escaped even from our most potent shRNA when applied as a sole inhibitor, whereas it failed to do so under concurrent pressure from all three shRNAs *in vitro* and *in vivo* (Figures 3 and 4). These results are highly reminiscent of previous findings for HIV and poliovirus[50–52] and thus add SARS-CoV-2 to the list of pathogenic RNA viruses for which combinatorial RNAi strategies are strictly indicated.[39] In this context, we note our finding that, of the three shRNAs tested in the passaging experiment, C8 resulted in escape in only one of three replicates, whereas mutational escape was observed in all three replicates with C12 and C3. This correlates well with the lower number of SNVs observed in the C8 target region compared with the C12 and C3 targets among the 365,255 SARS-CoV-2 isolates we assessed here (as of September 2021), including major VOCs (alpha [B.1.1.7], beta [B.1.351], gamma [P.1], and delta [B.1.617.2]). This further highlights the necessity to identify and target highly conserved sites in SARS-CoV-2 and illustrates the ensuing benefits for permanent *in vivo* ctrl. Most importantly, all three target sites for the C3, C8, and C12 shRNAs encoded in AAV-SAVIOR are also 100% conserved in the highly infectious omicron strain (B.1.1.529), which is currently rapidly replacing delta in many parts of the world and seems to be largely resistant to the anti-SARS-CoV-2 immunity triggered by current vaccines.

These notions are highly encouraging because they promise that future improved (see below) iterations of AAV-SAVIOR may thwart viral mutational escape in the human population and, thus, also enhance the efficacy of available vaccination regimens. The same concept is also pursued by monoclonal antibody cocktails that target multiple epitopes to prevent escape mutants.[53]

Also beneficial in this respect is the high versatility of our underlying AAV-TRISPR system, which permits simple and fast assembly of

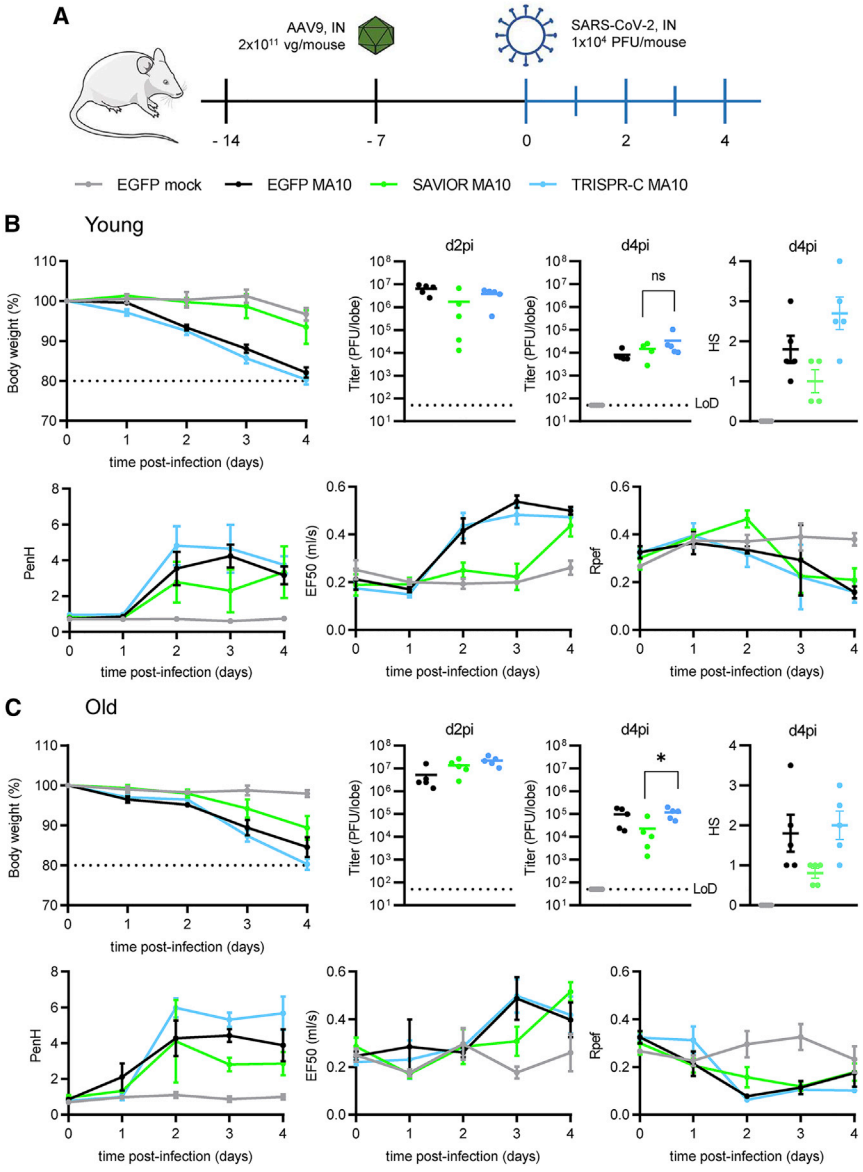

Figure 8. *In vivo* efficacy of AAV-SAVIOR in a mouse-adapted pathogenetic SARS-CoV-2-MA10 model

(A) Schematic of the study design. (B and C) Ten-week-old (B) or 1-year-old (C) mice were transduced intranasally (IN) with 2 × 10^{11} vg of AAV9-SAVIOR or with the TRISPR-C or EGFP ctrls 1 week prior to SARS-CoV-2-MA10 challenge (n = 5 animals per group). Multiple parameters, including physiological (body weight loss and airway obstruction scores [PenH, E50, and Repf]; means ± SD), pathological (lung hemorrhagic scores [HSs]), and virological parameters (lung titers 2 and 4 dpi; ns, non-significant; *p ≤ 0.05) were monitored and measured in the different experimental cohorts.

concatemerized scAAV vectors encoding combinations of up to three small RNAs via Golden Gate Assembly. Accordingly, unlike antibody therapeutic agents or vaccines that require several months for development, AAV-SAVIOR is a modular plug-and-play system with a significantly shorter engineering time. These small RNAs can comprise shRNAs as well as gRNAs, enabling combined expression of RNAi and CRISPR triggers from a single AAV vector, offering the future ability to target and inhibit SARS-CoV-2 and its host cell factors on the RNA and DNA levels, respectively. As exemplified here, this can include multiplexed targeting of three independent sites in the viral genome or transcripts, but one can also envision concurrent inhibition of virus and host genes. The latter should further increase the pressure on the virus and lower its chances to escape by mutation. Alternatively, it may also be rewarding to co-express three shRNAs against the identical target site but covering distinct point mutations to prevent viral breakthrough at this site. These looming efforts will greatly benefit from the multitude of algorithms and databases that are dedicated to identification of optimal RNAi and CRISPR targets in SARS-CoV-2 genomes and that take numerous design parameters into consideration, including conservation, accessibility, off-target potential in the host genome, and others.[23–26,28]

Clinical translation of the vector reported here should further benefit from, and be accelerated by, the long-standing experience in the field with its core components; namely, AAV capsids and RNAi cargos. This includes one of the strengths of the AAV vector system that we harnessed here: the ability to pseudotype cargos with a capsid mediating high and ideally specific transduction of a target cell or organ. In this work, we used the LK03 capsid to transduce cultured Vero E6 cells but then switched to AAV9 for transduction of mouse lungs *in vivo*. Although this selection was suggested by prior data showing the efficacy of this AAV isolate in the mouse lung,[54] it is clear that another capsid, likely a genetically engineered version,[55] may be required to improve the AAV-SAVIOR system and to enable its translation into higher species, including humans. In this respect, we note exciting recent work by Sims et al.,[56] who identified two AAV variants (hu68 and rh91) that potently transduce proximal airways in non-human primates when delivered by a mucosal atomization device. For use of AAV-SAVIOR as a first line of defense, it may be beneficial to pseudotype the vector with these capsids and to then apply it as a spray to the nose and upper airways to block entry of SARS-CoV-2 into the body at an early step. Moreover, using AAV barcoding and high-throughput *in vivo* screening technology,[57] we have recently confirmed the ability of other AAV capsids, such as AAV4 or a peptide display variant of AAV2,[58] to transduce mouse lungs from

intravenous delivery. If translatable to humans, this administration route could alleviate concerns in a therapeutic setting about physical barriers imposed by the thick mucosa in the lungs of individuals with COVID-19 or about SARS-CoV-2-containing aerosols that may be caused by use of nebulizers. However, intravenous AAV-SAVIOR delivery would also increase its exposure to the host immune system and may limit its efficacy. Although these different possibilities require experimental validation, we are not concerned that delivery of the vector reported here or of its descendants will become a bottleneck in the future, considering the manifold solutions offered by the AAV engineering field.[55]

Concurrent with optimization of capsid and delivery route, it is prudent to also learn and profit from the preclinical and clinical experience gathered with RNAi, including in an AAV context. In the past, AAV/RNAi vectors have been studied extensively as therapeutic agents for chronic liver infection with hepatotropic viruses, including treatment of HCV infection with a triple-shRNA construct (TT-033) in non-human primates.[40] In line with data in mice,[59] the same study reported dose-dependent toxicity in transduced hepatocytes because of high shRNA expression levels from RNA polymerase III promoters. Notably, subsequent promoter engineering to reduce shRNA levels lowered toxicity and enabled a phase I clinical trial with the optimized vector TT-034 as a first-in-human application of vector-delivered RNAi.[60] Therefore, future iterations of AAV-SAVIOR intended for use in humans should likewise benefit from engineering and optimization of the therapeutic cargo, including identification of promoters for the safest triple-shRNA expression. In the context of persistent viral infection, we also note reports of chronic or recurrent infection with SARS-CoV-2 in immunocompromised or immunodeficient individuals.[61–63] Although these may be amenable to treatment with convalescent plasma[63] or antiviral agents such as remdesivir,[64] they should also benefit from therapeutic application of AAV-SAVIOR, as supported by the robust viral clearance we observed here in chronically infected Caco-2 cells. It may be beneficial to include a genetic circuit in future vector generations that senses the presence of active or chronic viral replication or expression and temporally restricts vector activity. Finally, because the viral stage is transient and followed by an immune reaction that can cause severe pathology, it could be beneficial to arm AAV-SAVIOR with an immunomodulatory cargo or to supply this from a second vector to extend the initially short window for direct anti-viral targeting and to also control the detrimental host immune response at later stages.

In addition to outlining a path for technical improvements, our results also raise a series of related questions regarding the best parameters for clinical application, including kinetics and doses, that we could not address in this proof-of-concept study because of the scarcity and inherent limitations of *in vivo* SARS-CoV-2 models but that should be tackled by follow-up work. In particular, it will be seminal to more comprehensively characterize the *in vivo* persistence of triple-shRNA expression at multiple time points and the shRNA activity following a single vector administration to reveal the true potential of AAV-SAVIOR as a first-line-of-defense prophylactic agent. Along these lines, it will also be interesting to measure virus titers at earlier time points to identify beneficial effects that may be overwritten at later endpoints because of the high SARS-CoV-2 replication dynamics.

Within the aforementioned limits of *in vivo* studies on SARS-CoV-2, we acknowledge that the prophylactic effects observed in K18-hACE2 transgenic mice were moderate, probably for several reasons. One is that this mouse model requires a high virus input of 5×10^4 PFUs to induce pathogenesis in 100% of the animals, which is likely to overwhelm the antiviral capacity of our vector. Second, this mouse model is characterized by robust SARS-CoV-2 replication in the brain and ensuing morbidity and mortality. Although the AAV9 serotype is capable of crossing the blood-brain barrier from intravenous delivery in mice,[65] this was not expected in our study, where we used intranasal delivery. Accordingly, we observed no reduction in brain viral titers in treated K18-hACE2 mice. In contrast, the MA10 system provided more options for experimentation and analysis and also enabled use of 5-fold lower SARS-CoV-2 input doses. Consequently, we could better investigate the prophylactic effect of AAV-SAVIOR by measuring viral loads at two earlier timepoints (2 and 4 dpi), and we could also study two different age cohorts. AAV-SAVIOR pre-treatment yielded a trend toward reduced SARS-CoV-2 infection and related symptoms in young and old mice. The best results comprised protection from weight loss in young mice and a significant reduction in lung viral titers in older animals. A likely explanation for the stronger reduction of lung viral titers in older mice is the faster turnover rate of airway epithelial cells in young versus old mice.[66] Typically, the turnaround rate of airway epithelial cells is around 6 months in the trachea and 17 months in the lungs,[67] but these periods can be shorter in the case of injury. Importantly, in humans, this turnover rate is about 100 days to 1 year and can be even longer without injury, possibly providing a much wider prophylactic window.[67,68] We also clearly recognize a clinical benefit from alternative strategies, such as fast and transient siRNA delivery via nanoparticles,[21] especially in a therapeutic setting where long-term persistence of the RNAi cargo may not be needed. Vice versa, AAV-shRNA vectors offer a number of unique advantages, including the fact that they may require only a single dose versus multiple doses for siRNA or mRNA regimens. Moreover, as suggested by preclinical animal data, AAV capsid pseudotyping permits retargeting to other infected sites in the human body, such as the brain[69] or the intestine,[70] which may be far more difficult to reach with peripherally delivered nanoparticles, naked siRNAs, or mRNA complexes. As indicated above, this should ultimately allow us to target the AAV-SAVIOR system specifically and efficiently to the main lung cells types that are infected by SARS-CoV-2 in humans, alveolar type 2 (AT2) cells,[71,72] and boost the vector's antiviral efficacy.

Although the answers to these and other questions await further experimentation, this work already illustrates the benefits of multiplexed shRNA expression from pseudotyped AAV vectors as a prophylactic or therapeutic measure against SARS-CoV-2 infection and its clinical sequelae. Although multiple aspects of our first-generation

AAV-SAVIOR vector can and will be improved, the current iteration is sufficiently potent to inhibit viral replication and spread in cultured cells and in murine lungs with a single administration. Furthermore, it thwarted viral escape *in vitro* and *in vivo*, which we observed with traditional AAV vectors encoding a single shRNA and which is a major concern for any type of monotherapy. Combined with the general assets of AAVs, including apathogenicity, stability at ambient temperature, clinical safety, advanced manufacturing technology, and ease of engineering, this implies that AAV-SAVIOR holds significant potential as a new entry in our arsenal of measures to manage SARS-CoV-2 and other expected pandemics.

MATERIALS AND METHODS

Design, cloning, and multiplexing of anti-SARS-CoV-2 shRNAs

For the initial screening, shRNAs were directed against the *RdRp* and *N* genes of SARS-CoV-2 (NC_045512.2; shRNAs C1–19) or against the human ACE2 gene (NM_021804.3; shRNAs C20–22) and designed using the siRNA Wizard (https://www.invivogen.com/sirnawizard/index.php). All shRNAs were first cloned into single-shRNA vectors via Golden Gate Assembly (New England Biolabs, Ipswich, MA, USA). The recipient scAAV vector genome contained two inverted BsmBI sites under a U6 promoter as well as a GFP reporter controlled by a Rous sarcoma virus (RSV) promoter and a minimal polyadenylation site.[59] Forward and reverse shRNA oligos (Table S1) were ordered from Integrated DNA Technologies (Coralville, IA, USA) and annealed by mixing 2.5 μL of each oligo (100 μM) with 5 μL of NEBuffer 2 (NEB) and 40 μL of ddH_2O (double-distilled water), heating to 95°C for 5 min, and gradual cooling to 25°C over 15 min. For the assembly reaction, 15 fmol of recipient plasmid was mixed with 50 fmol of annealed oligos, 1 μL T4 DNA ligase buffer (NEB), 0.5 μL T4 DNA ligase (400 U/μL, NEB), and 0.5 μL of Esp3I (Thermo Scientific, Waltham, MA, USA) and filled to 10 μL with H_2O. Golden Gate Assembly was performed by cycling 25 times between 37°C for 2 min and 16°C for 3 min and finally inactivating the enzymes at 80°C for 10 min. Next, 5 μL of assembly mix was used for heat shock transformation of chemically competent DH5α cells, which were spread onto LB-agar plates containing 75 mg/L ampicillin. For selected clones, ITR integrity was assessed via BsaI/XmaI ctrl digestion, and correct insertion of shRNA oligos was validated via Sanger sequencing (Eurofins Genomics, Ebersberg, Germany) using the primer U6-forward 5′-ACCGCTCGAGCGAGTC CAACACCCGTGG-3′.

To multiplex three shRNAs in a single scAAV-TRISPR vector, a two-step Golden Gate Assembly protocol was applied as reported before.[43] In the first step, the selected oligos were cloned into three different donor vectors containing a U6, H1, or 7SK promoter via BsmBI-based Golden Gate Assembly as described above. After transformation of chemically competent bacteria, the cells were recovered for 1 h in 1 mL LB medium (37°C, 800 rpm) and plated onto LB-agar plates containing 25 μg/mL chloramphenicol. Correct insertions were validated by Sanger sequencing of selected clones using the M13Rev primer 5′-GGAAACAGCTATGACCATG-3′. The TRISPR donor plasmids contain inverted BbsI sites flanking each promoter-shRNA cassette. In a second Golden Gate Assembly step, these promoter-shRNA inserts were transferred to a recipient scAAV construct containing an acceptor site for the shRNA cassettes and a truncated *gfp* as stuffer. This yielded a final construct carrying the inserts U6-shRNA1/H1-shRNA2/7SK-shRNA3 in a defined order. For this reaction, 20 fmol of recipient plasmid was mixed with 20 fmol of each donor plasmid (U6/H1/7SK), 1 μL T4 DNA ligase buffer (NEB), 0.5 μL T4 DNA ligase (400 U/μL, NEB), and 0.5 μL of BbsI (Thermo Scientific) and filled to 10 μL with H_2O. Golden Gate Assembly cycling was performed as described above, and transformed chemically competent bacteria were plated on LB-agar plates with ampicillin. Sanger sequencing of selected clones was performed using the U6-forward primer or the GFP-reverse primer 5′-TCCTCCTTGA AGTCGATGC-3′.

Cell culture

HEK293T, Caco-2 (ATCC, HTB-37), and Vero E6 (ATCC, CRL 1586) cells were grown in Dulbecco's modified Eagle's medium (DMEM) with GlutaMAX (Life Technologies, Carlsbad, CA, USA) that was supplemented with 10% fetal bovine serum (fetal bovine serum [FBS]; Sigma-Aldrich, St. Louis, MO, USA) and 100 U/mL penicillin-streptomycin (Life Technologies). Cells were split every 2–4 days.

SARS-CoV-2 cultivation

The SARS-CoV-2 isolate Bavpat1/2020 was kindly provided by Prof. Christian Drosten and Dr. Mirko Cortese through the European Virology Archive (Ref-SKU 026V-03883) at passage 2.[73] Working stocks were generated by passaging the virus twice in Vero E6 cells. Infectious titer was determined by plaque assay on Vero E6 cells. SARS-CoV-2 MA10 stocks were also grown in Vero E6 cells and quantified via plaque assay.[49]

Human intestinal organoids

Human tissue was received from colon resections from the University Hospital Heidelberg. This study was carried out in accordance with the recommendations of the University Hospital Heidelberg with informed written consent from all subjects in accordance with the Declaration of Helsinki. All samples were received and maintained in an anonymous manner. The protocol was approved by the Ethics Commission of the University Hospital Heidelberg under protocol S-443/2017. Stem cells containing crypts were isolated and maintained as described previously.[47,74]

AAV production and purification

scAAV vectors were produced by polyethylenimine (PEI, linear, molecular weight [MW] 25,000; Polysciences, Hirschberg an der Bergstrasse, Germany) triple-transfection of HEK293T cells with (1) an scAAV vector plasmid containing one shRNA expression cassette for single-shRNA vectors, three shRNAs for TRISPR constructs (including SAVIOR), or a GFP expression cassette for ctrl vectors, all flanked by one AAV2 and one truncated AAV4 ITR (together yielding the scAAV genotype)'[59] (2) an AAV helper plasmid containing AAV *rep* and *cap* genes; and (3) an adenoviral helper plasmid.[75]

AAV helper plasmids and the encoded *cap* gene were adapted based on the targeted cell type.

For the initial screens of the full shRNA panel in Vero E6 cells, vectors were produced at small scale as "crude cell lysates" in a 6-well format as reported before,[76] using the LK03 capsid.[36] Briefly, 3×10^6 HEK293T cells were seeded in 6-well plates in 2 mL full medium. One day after seeding, cells were transfected with 870 ng of each plasmid using a PEI mix containing 22 μL of PEI, 27 μL H_2O, and 49 μL 300 mM NaCl (total volume, 98 μL), which was then combined with the DNA mix at a total of 98 μL (DNA diluted in 49 μL H_2O and 49 μL 300 mM NaCl). After vortexing and incubation for 10 min at room temperature (RT), the combined mix was added dropwise to each well. Forty-eight hours after transfection, the medium was exchanged with 1 mL PBS (Life Technologies), and cells were harvested by pipetting. After centrifugation at 1,500 × *g* for 10 min, the cell pellet was resuspended in 400 μL PBS and lysed by five freeze-thaw cycles (liquid nitrogen/37°C) and 1 min of sonication. Cell debris was removed by centrifuging the lysate for 10 min at 16,000 × *g* and discarding the pellet.

For subsequent experiments in cell culture, AAV production was scaled up to five 15-cm dishes per construct using the LK03 capsid for transduction of Vero E6 cells and gut organoids and AAV6 for transduction of Caco-2 cells. 4×10^6 HEK293T cells were seeded per 15-cm plate 2 days prior to triple transfection. A DNA mix was prepared, containing 74 μg of each plasmid (shRNA vector, AAV helper, and adenoviral helper) in 4 mL H_2O and 4 mL 300 mM NaCl. Next, a PEI mix was prepared, containing 2 mL PEI, 2.2 mL H_2O, and 4 mL 300 mM NaCl. Both mixes were combined, vortexed, and incubated at RT for 10 min before being added dropwise to the cells. Transfected cells were harvested 72 h later, pelleted by 15-min centrifugation at 800 × *g*, and resuspended in 5 mL Benzonase buffer (150 mM NaCl, 50 mM Tris-HCl, 2 mM $MgCl_2$ [pH 8.5]) before being lysed with five consecutive freeze-thaw cycles (liquid nitrogen and water bath at 37°C). Lysates were incubated with 75 U/mL Benzonase (Merck, Darmstadt, Germany) for 1 h at 37°C while inverting the tubes every 10 min. Cell debris was cleared by two rounds of centrifugation at 4,000 × *g* for 15 min and discarding the pellet. All vectors were purified via iodixanol gradient density centrifugation. Each lysate was filled to 7 mL and loaded into ultracentrifugation tubes (Seton Scientific, Petulama, CA, USA) through a Pasteur pipette. This was underlaid with 1.5 mL each of 15%, 25%, 40%, and, finally, 60% iodixanol solution. The sealed tubes were centrifuged at 50,000 rpm (4°C) for 2 h in an Optima L-90K ultracentrifuge using a 70.1 Ti rotor (Beckman Coulter, Brea, CA, USA). Finally, the 40% iodixanol phase containing full capsids was extracted through a needle, aliquoted, and stored at −80°C.

For mouse experiments, the AAV9 capsid was used, and vectors were produced in 40 15-cm dishes per construct. They were purified via iodixanol gradients as described above but using lysate from 20 plates per gradient tube; i.e., two gradients per sample. Each purified vector sample (in 40% iodixanol) was then filled to 15 mL with PBS and concentrated to approximately 500 μL using Amicon Ultra-15 centrifugation columns (Merck) by centrifugation at 1,000 × *g*. The columns were briefly inverted every 5 min to prevent clogging of the filter membrane.

AAV titration by quantitative real-time PCR

Concentrations of viral genomes in purified AAV stocks were determined by quantitative real-time PCR as reported previously,[77] using the GFP-forward 5′-ATCTTCTTCAAGGACGACG-3′ and GFP-reverse 5′-TCCTCCTTGAAGTCGATGC-3′ primers with the GFP probe 5′-FAM-ACGACGGCAACTACA-BHQ1-3′. Viral capsids were lysed by incubating 10 μL of 1:10 diluted purified vector in 10 μL TE buffer with 20 μL 1 M NaOH at 56°C for 30 min. The alkaline lysis reaction was stopped with 38 μL 2 M HCl and filled to 1 mL with H_2O. Per sample, three 10-μL qPCR reactions were prepared as a 3.5-fold master mix containing 17.5 μL Sensimix II (Sensimix II probe kit; Meridian Bioscience, Cincinnati, OH, USA), 0.4 μM of each forward and reverse primer, 0.3 μM probe, and 5 μL of lysed vector sample or diluted reference GFP plasmid (1:10 dilutions from 5×10^8 to 5×10^3 copies per reaction for the standard curve). The qPCR was run in a Rotor Gene 6000 (QIAGEN, Hilden, Germany) by first heating to 95°C for 10 min and then cycling 40 times between 95°C for 10 s and 60°C for 20 s. Afterward, a linear regression was performed for the standard curve in the RotorGene 6000 Series 1.7 software. The resulting copy number per reaction was corrected by multiplication with 7 (dilution within the qPCR reaction) × 10 (pre-dilution of vector) × 100 (dilution during alkaline lysis) × 100 (result per mL).

AAV transduction and SARS-CoV-2 infection of cultured cells

Prior to transduction, Vero E6 cells were seeded in 96- or 48-well plates with approximately 6,400 cells (in 100 μL medium) or 5×10^5 cells per well (in 500 μL medium), respectively. AAV vectors were immediately added to each well at a multiplicity of infection (MOI) of 10^5 vectors per cell, diluted in full medium to 10 μL (for 96-well plates) or 50 μL (for 48-well plates). Three days after transduction, cells were infected with SARS-CoV-2 at an MOI of 3 (BavPat1 strain, passage 3). For the viral escape experiment, 50 μL supernatant from cells infected 1 day earlier was added to freshly AAV-transduced cells. This was continued for a total of eight passages.

Evaluation of ACE2 knockdown with shRNA C20, C21, or C22 vectors

Single-shRNA AAV-LK03 vectors encoding shRNA ctrl, C20, C21, or C22 were produced, purified, and titrated as described before. Vero E6 cells were seeded in a 24-well format at a density of 1×10^5 cells per well and immediately transduced at an MOI of 1×10^5 (one vector per well, n = 3 wells per vector). Three days later, cellular RNA was extracted using the RNeasy Mini Kit (QIAGEN) and converted into cDNA using the High Capacity cDNA Synthesis Kit (Applied Biosystems, Waltham, MA, USA). Quantitative reverse transcriptase PCR of cDNA was performed for ACE2 as well as the housekeeper glyceraldehyde 3-phosphate dehydrogenase (GAPDH) with the StepOnePlus Real-Time PCR System (Thermo Fisher) using iTaq Universal SYBR Green Supermix (Bio-Rad, Hercules, CA, USA). The primer

sets used for quantitative reverse transcriptase PCR were GAPDH_fw (5′-ACCCACTCCTCCACCTTTGAC-3′) and GAPDH_rev (5′-TGTTGCTGTAGCCAAATTCGTT-3′) for GAPDH and hACE2_fw (5′-TCCATTGGTCTTCTGTCACCCG-3′) and hACE2_rev (5′-AGACCATCCACCTCCACTTCTC-3′) for ACE2. Each reaction was performed in duplicates, of which the mean Ct value was used for further analysis. The difference in ACE2 expression was quantified by first normalizing ACE2 Ct values to GAPDH for each replicate (i.e., ΔCt) and then normalizing the active shRNA (C20–C22) conditions to shRNA ctrl (i.e., ΔΔCt). The fold change in expression was finally calculated using the $2^{\Delta\Delta Ct}$ method. Statistical significance was evaluated using a one-way ANOVA.

Luciferase knockdown assays with psiCheck-2 reporters

To analyze shRNA knockdown efficiency in a luciferase reporter context, a triple binding site for the C8, C12, and C3 shRNAs was designed as forward (5′-tcgagGTGATAGAGCCATGCCTAACActcacGACTGAGACTGACCTTACTAActagaGACAAGGCGTTCCAATTAACAgc-3′) and reverse oligonucleotides (5′-ggccgcTGTTAATTGGAACGCCTTGTCtctagTTAGTAAGGTCAGTCTCAGTCgtgagTGTTAGGCATGGCTCTATCACc-3′; Merck; lowercase letters are overhangs or spacers). These were annealed and cloned into the 3′ UTR of *Renilla* luciferase in psiCheck-2 (Promega, Madison, WI, USA) using XhoI and NotI restriction sites. To study knockdown of mutated shRNA binding sites, point mutations from escape mutants (Figure 4A) were selected for C8 (mutated binding site 8*: 5′-GTGATAGGGCCATGCCTAACA-3′), C12 (mutated binding site 12*: 5′-GACTGAGATTGACCTTACTAA-3′), and C3 (mutated binding site 3*: 5′-GACAAGGCGTCCCAATTAACA-3′), and permutations with one, two, or three mutated binding sites were cloned by using oligonucleotides according to the design above.

Dual luciferase assays were conducted by first seeding 12,500 HEK293T cells per well in a 96-well format. After 24 h, cells in each well were co-transfected (n = 3 biological replicates) with 10 ng of reporter plasmid and 100 ng of effector plasmid using Lipofectamine 2000 (Thermo Fisher, 0.4 μL per well). The effectors used were single-shRNA constructs for shRNA ctrl (non-targeting control), C8, C12, or C3; or TRISPR constructs expressing three shRNAs each. Cells were lysed 4 days after transfection using passive lysis buffer, and luminescence was measured in a GloMax Navigator microplate luminometer using the Dual-Luciferase Reporter Assay System (all from Promega). Relative luminescence units (RLUs) were calculated by dividing *Renilla* by firefly luminescence values, and they were subsequently normalized to the appropriate ctrl condition (TRISPR-C for the TRISPR panel and shRNA ctrl knockdown of mutated binding sites).

Analysis of vector genome integrity

To analyze the genome integrity of scAAV vectors, 5×10^{11} AAV particles (vector genomes as quantified by qPCR) were treated with Proteinase K (QIAGEN) for 30 min at 56°C. Next, vector DNA was extracted using the DNeasy Blood & Tissue Kit (QIAGEN), mixed with 6× purple gel loading dye (NEB), and loaded next to the 1 Kb Plus DNA Ladder (Thermo Fisher) onto a native 1% agarose gel stained with ethidium bromide (Roth, Karlsruhe, Germany). Electrophoresis was performed in 1× TAE (tris-acetate-EDTA) buffer at 120 V for 30 min.

Infection of colon organoids in 2D

8-well glass-bottom chambers (ibidi, Graefling, Germany) were coated with 2.5% human collagen in water for 1 h prior to organoid seeding. Organoids were collected at a ratio of 100 organoids per well of a 48-well plate. Collected organoids were spun at 450 × *g* for 5 min, and the supernatant was removed. Organoids were washed with cold 1× PBS and spun at 450 × *g* for 5 min. PBS was removed, and organoids were digested with 0.05% Trypsin-EDTA (Life Technologies) for 5 min at 37°C. Digestion was stopped by addition of serum-containing medium. Organoids were spun at 450 × *g* for 5 min, and the supernatant was removed before organoids were resuspended in normal growth medium at a ratio of 250 μL medium per well. The collagen mixture was removed from the ibidi chambers, and 250 μL of organoids were added to each well. Forty-eight hours after seeding, the medium was removed and replaced with differentiation medium for 4 days. Following organoid differentiation, organoids were transduced with AAV vectors at an MOI of 10^5. Three days after transduction, the medium was removed, and transduced organoids were infected with SARS-CoV-2 (BavPat1, passage 3) at an MOI of 1 for 1 h. Following infection, virus was removed, cells were washed with 1× PBS, and differentiation medium was replaced. Twenty-four hours after infection, supernatants and RNA were harvested.

Infection of chronically infected Caco-2 cells

500,000 Caco-2 cells were seeded into a 6-well plate and infected with SARS-CoV-2 at an MOI of 1. Forty-eight hours after infection, the medium was replaced with fresh medium. Caco-2 cells were maintained in culture for 8 weeks with regular observation by qPCR and immunofluorescence (IF) for SARS-CoV-2 replication. Caco-2 cells continued to grow and secrete SARS-CoV-2 over the time course. Eight weeks after infection, 100,000 chronically infected cells were seeded into 24-well plates. Cells were transduced with AAV vectors at an MOI of 10^5. 2, 3, and 5 days after transduction, medium was harvested for virus titration, and RNA was collected and processed as described below.

RNA isolation, cDNA preparation, and quantitative reverse transcriptase PCR of SARS-CoV-2-infected cells

RNA was harvested from cells using the RNeasy RNA extraction kit (QIAGEN) following the manufacturer's instructions. cDNA was made using iSCRIPT reverse transcriptase (Bio-Rad) from 250 ng of total RNA according to the manufacturer's instructions. Quantitative reverse transcriptase PCR was performed using iTaq SYBR Green (Bio-Rad) following the manufacturer's instructions. HPRT1 (primers for 5′-CCTGGCGTCGTGATTAGTGAT-3′ and 5′-AGACGTTCAGTCCTGTCCATAA-3′) was used as a housekeeper. SARS-CoV-2 was detected with primers for 5′-GCCTCTTCTGTTCCTCATCAC-3′ and rev 5′-AGACAGCATCACCGCCATTG-3′.

Indirect IF assay of SARS-CoV-2-infected cells

Twenty-four hours after infection, cells were fixed in 4% paraformaldehyde (PFA) for 20 min at RT. Cells were washed and permeabilized in 0.5% Triton X-100 for 15 min at RT. The primary antibody against dsRNA (clone J2, catalog number 10010200; SCICONS, Szirák, Hungary) was diluted 1:1,000 in PBS and incubated for 1 h at RT. Cells were washed in 1× PBS three times and incubated with 1:10,000 dilutions of secondary antibodies (IRDye 800CW anti-mouse immunoglobulin G [IgG], catalog number 926-32212; LI-COR Biosciences, Lincoln, NE, USA) and Draq5 (a DNA dye, catalog number 4ab108410, Abcam, Cambridge, UK) for 45 min at RT. Then cells were washed again in 1× PBS three times and maintained in PBS. Cells were imaged using an Odyssey (LI-COR Biosciences) reader.

$TCID_{50}$ assay of *de-novo*-produced SARS-CoV-2

20,000 Vero E6 cells were seeded per well into a 96-well dish. Twenty-four hour later, 100 µL of harvested supernatant was added to the first well. Seven 1:10 dilutions were made (all samples were in triplicate). Infection was allowed to proceed for 24 h before cells were fixed in 4% PFA for 20 min at RT. PFA was removed, and cells were washed twice in 1× PBS and then permeabilized for 10 min at RT in 0.5% Triton X-100. Cells were blocked in a 1:2 dilution of blocking buffer (LI-COR Biosciences) for 30 min at RT and then stained with 1:1,000 diluted anti-dsRNA antibody (clone J2, catalog number 10010200, SCICONS) for 1 h at RT. Cells were washed three times with 0.1% Tween in PBS. Secondary antibody (IRDye 800CW anti-mouse IgG, catalog number 926-32212, LI-COR Biosciences) and the DNA dye Draq5 (Abcam) were diluted 1:10,000 in blocking buffer and incubated for 1 h at RT. Cells were washed three times with 0.1% Tween/PBS and finally imaged in 1× PBS on an Odyssey (LI-COR Biosciences) imager.

Sanger sequencing analysis of mutated shRNA binding sites

RNA was extracted from cell supernatants of passages 1, 3, 5, and 7 from the viral escape experiment using the RNeasy Mini Kit (-QIAGEN) by following the manufacturer's instructions and eluting with 30 µL nuclease-free H_2O. The entire eluate was subjected to reverse transcription using the High Capacity cDNA Synthesis Kit (Applied Biosystems). Per cDNA sample, two fragments were PCR amplified separately from (1) the SARS-CoV-2 *RdRp* gene in ORF1ab containing the C8 and C12 shRNA binding sites and (2) from the *N* gene containing the C3 shRNA binding site. For the *RdRp* gene, amplification was achieved with the primer set C8C12_Rseq_fw 5′-GCAAATTCTATGGTGGTTGGCA-3′ and C8C12_Rseq_rev 5′-CCGGCCCCTAGGATTCTTGA-3′, whereas the *N* gene fragment was amplified with primers C3_Nseq_fw 5′-AGAATGGAGAACGCAGTGGG-3′ and C3_Nseq_rev 5′-GCTTCTGGCCCAGTTCCTAG-3′. Each PCR reaction contained 0.5 µL of Phusion Hot Start II High Fidelity DNA polymerase (Thermo Scientific) as well as 10 µL Phusion HS II buffer, 1 µL deoxynucleotide (dNTP) solution mix (NEB), 0.25 µL of each of the respective forward and reverse primers (100 µM stock; final concentration, 0.5 µM), 5 µL cDNA template, and 35 µL nuclease-free H_2O (QIAGEN). Amplification was performed with an initial denaturation at 98°C for 30 s, followed by 40 cycles of denaturation (98°C, 15 s), annealing (60°C, 30 s) and elongation (72°C, 30 s), and a final 5-min elongation at 72°C. PCR products were prepared for Sanger sequencing by mixing 1 µL amplicon with 8.75 µL H_2O and 0.25 µL of the respective forward or reverse amplification primer (100 µM stock; final concentration, 2.5 µM), and then sequenced with the Eurofins Genomics Sanger sequencing service.

Experiments in hACE-2-transgenic and wild-type ctrl mice

Animal experiments at the University of Heidelberg were carried out in accordance with the standards approved by the central animal facility of the University of Heidelberg (G-96/20). Male heterozygous K18-hACE2 (B6.Cg-Tg(K18-ACE2)2Prlmn/J) mice in the C57BL/6 background were obtained from The Jackson Laboratory (stock number 034860), imported via embryo transfer into the general animal facility at the University of Heidelberg, and bred heterozygously with wild-type C57BL/6 females. The genotype of the mice was assessed by PCR on total genomic DNA from ear punches using primers that distinguish between homozygous and heterozygous K18-hACE2 transgenic and wild-type mice: primer 53437, 5′-GACCCCTGAGGGTTTCATATAG-3′; primer 53438, 5′-CACCAACACAGTTTCCCAAC-3′; and primer 53439, 5′-AAGTTGGAGAAGATGCTGAAAGA-3′. Mice were kept at 22°C ± 2°C at 45%–65% relative humidity with a 12-h light/dark cycle and fed *ad libitum* with Altromin Rod 16 or Rod 18. Cages were supplemented with ABBEDD LT-E−001 bedding and Crincklets nest pads. At the general animal facility, mice were kept in conventional type II cages with filter tops. At the age of 14 weeks, 2 days before initiation of the experiment, mice were transferred into the biosafety level 3 (BSL3) area, kept in individually ventilated cages (Green Line; Tecniplast, Buguggiate, Italy) under negative pressure, and provided with DietGel Boost (ClearH_2O, Westbrook, ME, USA) to reduce the severity of weight loss upon infection.

Male K18-hACE2 transgenic mice and wild-type littermates were transduced with AAV9 vectors intranasally under short-term anesthesia with 5% isoflurane, by applying 2×10^{11} vg in a total volume of 50 µL PBS to both nostrils. Seven days later, mice were infected via both nostrils with 5×10^4 PFUs of SARS-CoV-2 BavPat1 in a total volume of 50 µL DMEM without supplements. The SARS-CoV-2 isolate Bavpat1/2020 was kindly provided by Prof. Christian Drosten and Mirko Cortese through the European Virology Archive (Ref-SKU 026V-03883) at passage 2.[73] Working stocks were generated by passaging the virus twice in Vero E6 cells. Mice were visually inspected every day to assess disease score and body weight. Transgenic mice were harvested when they qualified for euthanasia by reaching the maximum disease score of 20 (Table S4). The respective wild-type animals were always harvested in parallel. For organ harvest, mice were deeply anesthetized with 5% isoflurane and killed by cervical dislocation. Lungs and brains were collected and directly transferred into pre-cooled 2-mL homogenization tubes filled with 1.4-mm ceramic beads (Omnilab, Bremen, Germany) and 500 µL DMEM without supplements. Tissue was homogenized for 1 min at 4 m/s using a Bead Ruptor 12A (Omnilab) and centrifuged at 4°C

for 1 min at maximum speed, and then the supernatant was transferred into a fresh tube.

Samples for qPCR and the plaque assay were generated from cleared organ homogenates. For qPCR, 50 μL of cleared organ homogenate was mixed with 350 μL lysis buffer LBP (Macherey-Nagel, Düren, Germany) and stored at −80°C until RNA extraction. RNA isolation (NucleoSpin RNA Plus Mini Kit, Macherey-Nagel), cDNA synthesis (high-capacity cDNA reverse transcription kit, Thermo Scientific), and quantitative reverse transcriptase PCR were performed as described previously.[73] Briefly, cDNA samples were diluted 1:15 and used for qPCR with iTaq Universal SYBR Green Master Mix (Bio-Rad) using the primers SARS-CoV-2-N Fwd 5′-GCCTCTTCTCGTTCCTCATCAC-3′ and SARS-CoV-2-N Rev 5′-AGCAGCATCACCGCCATTG-3′. Relative abundance of viral RNA was determined by correcting cycle threshold values for PCR efficiency. A standard of known concentration was included on each plate to calculate absolute viral RNA copy numbers from a standard curve.

Plaque assays were performed as described previously.[78] Here, Vero E6 cells were infected with serial dilutions of infectious supernatants or cleared organ homogenates. After infection for 1–3 h, the supernatant was removed, and cells were incubated with minimum essential medium (MEM) containing 0.8% carboxymethylcellulose (Sigma-Aldrich). 72 h after infection, cells were fixed with 10% PBS-buffered formaldehyde (37°C for 30 min), followed by immersion of the whole plates in 6% H_2O-diluted formaldehyde (37°C for 30 min) and staining for 15–30 min with 2.3% crystal violet solution (Sigma-Aldrich). After washing and drying the stained plates, plaques were counted manually, and virus titers were calculated.

Transduction of BALB/c mice with AAV9 vectors for infection with SARS-CoV-2-MA10 or wild-type SARS-CoV-2

Female BALB/c mice used in SARS-CoV-2-MA10 infection experiments were obtained from Envigo (Indianapolis, IN, USA; BALB/cAnNHsd, strain 047) and housed at the University of North Carolina at Chapel Hill until AAV transduction. The generation of recombinant SARS-CoV-2 MA and in vivo passaging was approved for use under BSL3 conditions by the University of North Carolina at Chapel Hill Institutional Review Board (UNC-CH IBC) and by a Potential Pandemic Pathogen Care and Oversight committee at the National Institute of Allergy and Infectious Diseases (NIAID). All animal work was approved by Institutional Animal Care and Use Committee at University of North Carolina at Chapel Hill according to guidelines outlined by the Association for the Assessment and Accreditation of Laboratory Animal Care and the U.S. Department of Agriculture. All work was performed with approved standard operating procedures and safety conditions for SARS-CoV-2. AAV9-SAVIOR, scrambled gRNA ctrl, or EGFP vectors were administered at 2×10^{11} vg via the intranasal route 1 or 2 weeks prior to SARS-CoV-2-MA10 challenge. Then the animals were moved into the BSL3 laboratory, where they were acclimated until the start of the challenge experiment. Mice were anesthetized with ketamine/xylazine prior to intranasal infection with 1×10^4 PFUs of SARS-CoV-2 MA10 diluted in PBS. Infection-related parameters, such as weight loss and morbidity, were monitored daily. Lung function was recorded via whole-body plethysmography (WBP; DSI Buxco respiratory solutions, St. Paul, MN, USA) for the indicated cohorts and time points as described previously[79] and analyzed using FinePointe (DSI, New Brighton, MN, USA), to determine PenH and Repf (airway resistance of the mouse lung) as well as EF50 (exhalation flow rate).

Ctrl as well as SARS-CoV-2-MA10-infected mice were euthanized via isoflurane overdose and harvested at the indicated time points. Caudal right lung lobes were collected for measurement of HSs (ranging from 0–5 with 0.5 increments, as determined by the overall edema of the mouse lungs) and viral load analysis via plaque assay, for which tissue was homogenized in 1 mL of PBS and glass beads. Dilution series of supernatants were used to infect monolayers of Vero E6 cells, which were stained with Neutral Red dye 72 h after infection to visualize plaques.

Bioinformatics analysis of mutations in known SARS-CoV-2 genomes

As of September 2021, a total of 365,255 full-length SARS-CoV-2 genomes were acquired from GenBank (http://www.ncbi.nlm.nih.gov). These genome sequences were mapped against the SARS-CoV-2 reference genome (GeneBank: NC_045512.2) by utilizing BWA (v.0.7.17).[80] Variant calling was performed by using SAMtools (v.1.11) and BCFtools (v.1.11).[81] Detected genomic variants were annotated by SnpEff (v.4.5.1)[82] using a locally built annotation database corresponding to the NC_045512.2 reference acquired from the NCBI database as a GFF (general feature format) file. Computations were performed on a high-performance cluster running the Slurm Workload Manager using 16 CPUs and 8 GB memory. Visualization of the genome-wide mutation landscape was performed in R (v.3.6.3).[83] The dataset was split into 20 subsets and processed in parallel because of the computational limitations of R for character strings. Average identity (percent) of 40,000 randomly picked, aligned, full-length SARS-CoV-2 genomes per genomic site was calculated as the ratio of the number of genomes with mutation to the total number of genomes in the dataset (40,000). Scripts used for variant calling, annotation, and visualization are available from the corresponding author upon request.

Statistical analysis

For quantification of p values, the GraphPad Prism software package was used to conduct a two-tailed unpaired t test or Kruskal-Wallis test with Dunn's multiple comparisons test. p values are indicated as follows: ns, non-significant; *$p \leq 0.05$; **$p \leq 0.01$; ***$p \leq 0.001$; ****$p \leq 0.0001$. In Figure 7, transgenic animals were compared among each other, as were wild-type animals and animals that received the same treatment.

SUPPLEMENTAL INFORMATION

Supplemental information can be found online at https://doi.org/10.1016/j.ymthe.2022.01.024.

ACKNOWLEDGMENTS

D.G. and O.T.F. were supported by the German Research Foundation (DFG) through the Cluster of Excellence CellNetworks (EXC81) as well as the DFG Collaborative Research Center SFB1129 (Projektnummer 240245660). D.G. also acknowledges funding from DFG TRR179 (Projektnummer 272983813) as well as the German Center for Infection Research (DZIF; Bundesministerium für Bildung und Forschung [BMBF]; TTU-HIV 04.819). D.G. and O.T.F. acknowledge support from the Sonderfördermaßnahme COVID-19 des Landes Baden-Württemberg. R.S.B. has received support from the National Institutes of Health (AI149644 and AI108197). This project received support from NIH grant AI151797 (to R.S.B.). L.V.T. is the recipient of the Pfizer NCBiotech Distinguished Postdoctoral Fellowship in Gene Therapy. S.B. was supported by DFG project numbers 415089553 (Heisenberg program), 240245660 (SFB1129), 278001972 (TRR186), and 272983813 (TRR179); the state of Baden-Württemberg (AZ: 33.7533.-6-21/5/1); the BMBF (01KI20198A); and within the Network University Medicine – Organo-Strat COVID-19. M.L.S. was supported by the BMBF (01KI20239B) and DFG project 416072091. We thank various members of the Grimm group for critical reading of the manuscript.

AUTHOR CONTRIBUTIONS

J.B., M.L.S., S.B., and D.G. initially conceived this project. J.B., A.G., and D.G. designed the anti-SARS-CoV-2 shRNAs tested in this work. J.B., L.V.T., S.R.L., B.S., A.W., I.A., and M.L.S. performed and analyzed experiments. O.M. performed all bioinformatics analyses. E.W. provided critical support for AAV preparations. K.B. screened suitable AAV variants for the cell culture experiments. L.V.T., O.T.F., R.S.B., S.B., and D.G. supervised the work in their laboratories. All authors were involved in preparation of figures and text, and all approved the final manuscript.

DECLARATION OF INTERESTS

D.G. is a co-founder and shareholder of AaviGen GmbH. S.R.L. and R.B.S have filed a patent application for SARS-CoV-2-MA10. K.B. is an employee of AskBio GmbH.

REFERENCES

1. Baden, L.R., El Sahly, H.M., Essink, B., Kotloff, K., Frey, S., Novak, R., Diemert, D., Spector, S.A., Rouphael, N., Creech, C.B., et al. (2020). Efficacy and safety of the mRNA-1273 SARS-CoV-2 vaccine. N. Engl. J. Med. *384*, 403–416.

2. Logunov, D.Y., Dolzhikova, I.V., Shcheblyakov, D.V., Tukhvatulin, A.I., Zubkova, O.V., Dzharullaeva, A.S., Kovyrshina, A.V., Lubenets, N.L., Grousova, D.M., Erokhova, A.S., et al. (2021). Safety and efficacy of an rAd26 and rAd5 vector-based heterologous prime-boost COVID-19 vaccine: an interim analysis of a randomised controlled phase 3 trial in Russia. Lancet *397*, 671–681.

3. Polack, F.P., Thomas, S.J., Kitchin, N., Absalon, J., Gurtman, A., Lockhart, S., Perez, J.L., Pérez Marc, G., Moreira, E.D., Zerbini, C., et al. (2020). Safety and efficacy of the BNT162b2 mRNA covid-19 vaccine. N. Engl. J. Med. *383*, 2603–2615.

4. Voysey, M., Clemens, S.A.C., Madhi, S.A., Weckx, L.Y., Folegatti, P.M., Aley, P.K., Angus, B., Baillie, V.L., Barnabas, S.L., Bhorat, Q.E., et al. (2021). Safety and efficacy of the ChAdOx1 nCoV-19 vaccine (AZD1222) against SARS-CoV-2: an interim analysis of four randomised controlled trials in Brazil, South Africa, and the UK. Lancet *397*, 99–111.

5. Pardi, N., and Weissman, D. (2020). Development of vaccines and antivirals for combating viral pandemics. Nat. Biomed. Eng. *4*, 1128–1133.

6. Beigel, J.H., Tomashek, K.M., Dodd, L.E., Mehta, A.K., Zingman, B.S., Kalil, A.C., Hohmann, E., Chu, H.Y., Luetkemeyer, A., Kline, S., et al. (2020). Remdesivir for the treatment of covid-19 — final report. N. Engl. J. Med. *383*, 1813–1826.

7. WHO Solidarity Trial Consortium (2020). Repurposed antiviral drugs for covid-19 — interim WHO solidarity trial results. N. Engl. J. Med. *384*, 497–511.

8. Chen, P., Nirula, A., Heller, B., Gottlieb, R.L., Boscia, J., Morris, J., Huhn, G., Cardona, J., Mocherla, B., Stosor, V., et al. (2020). SARS-CoV-2 neutralizing antibody LY-CoV555 in outpatients with covid-19. N. Engl. J. Med. *384*, 229–237.

9. Weinreich, D.M., Sivapalasingam, S., Norton, T., Ali, S., Gao, H., Bhore, R., Musser, B.J., Soo, Y., Rofail, D., Im, J., et al. (2020). REGN-COV2, a neutralizing antibody cocktail, in outpatients with covid-19. N. Engl. J. Med. *384*, 238–251.

10. Alouane, T., Laamarti, M., Essabbar, A., Hakmi, M., Bouricha, E.M., Chemao-Elfihri, M.W., Kartti, S., Boumajdi, N., Bendani, H., Laamarti, R., et al. (2020). Genomic diversity and hotspot mutations in 30,983 SARS-CoV-2 genomes: moving toward a universal vaccine for the "confined virus"? Pathogens *9*, 829.

11. Badua, C., Baldo, K.A.T., and Medina, P.M.B. (2020). Genomic and proteomic mutation landscapes of SARS-CoV-2. J. Med. Virol. *93*, 1702–1721.

12. Davies, N.G., Abbott, S., Barnard, R.C., Jarvis, C.I., Kucharski, A.J., Munday, J.D., Pearson, C.A.B., Russell, T.W., Tully, D.C., Washburne, A.D., et al. (2021). Estimated transmissibility and impact of SARS-CoV-2 lineage B.1.1.7 in England. Science *372*, eabg3055.

13. Korber, B., Fischer, W.M., Gnanakaran, S., Yoon, H., Theiler, J., Abfalterer, W., Hengartner, N., Giorgi, E.E., Bhattacharya, T., Foley, B., et al. (2020). Tracking changes in SARS-CoV-2 spike: evidence that D614G increases infectivity of the COVID-19 virus. Cell *182*, 812–827.e19.

14. Oude Munnink, B.B., Sikkema, R.S., Nieuwenhuijse, D.F., Molenaar, R.J., Munger, E., Molenkamp, R., van der Spek, A., Tolsma, P., Rietveld, A., Brouwer, M., et al. (2020). Transmission of SARS-CoV-2 on mink farms between humans and mink and back to humans. Science *371*, 172–177.

15. Plante, J.A., Liu, Y., Liu, J., Xia, H., Johnson, B.A., Lokugamage, K.G., Zhang, X., Muruato, A.E., Zou, J., Fontes-Garfias, C.R., et al. (2020). Spike mutation D614G alters SARS-CoV-2 fitness. Nature *592*, 116–121.

16. Wibmer, C.K., Ayres, F., Hermanus, T., Madzivhandila, M., Kgagudi, P., Oosthuysen, B., Lambson, B.E., de Oliveira, T., Vermeulen, M., van der Berg, K., et al. (2021). SARS-CoV-2 501Y.V2 escapes neutralization by South African COVID-19 donor plasma. Nat. Med. *27*, 622–625.

17. Starr, T.N., Greaney, A.J., Addetia, A., Hannon, W.W., Choudhary, M.C., Dingens, A.S., Li, J.Z., and Bloom, J.D. (2021). Prospective mapping of viral mutations that escape antibodies used to treat COVID-19. Science *371*, 850.

18. Uludağ, H., Parent, K., Aliabadi, H.M., and Haddadi, A. (2020). Prospects for RNAi therapy of COVID-19. Front. Bioeng. Biotechnol. *8*, 916.

19. Wu, C.-J., Huang, H.-W., Liu, C.-Y., Hong, C.-F., and Chan, Y.-L. (2005). Inhibition of SARS-CoV replication by siRNA. Antivir. Res. *65*, 45–48.

20. Li, B.-j., Tang, Q., Cheng, D., Qin, C., Xie, F.Y., Wei, Q., Xu, J., Liu, Y., Zheng, B.-j., Woodle, M.C., et al. (2005). Using siRNA in prophylactic and therapeutic regimens against SARS coronavirus in Rhesus macaque. Nat. Med. *11*, 944–951.

21. Idris, A., Davis, A., Supramaniam, A., Acharya, D., Kelly, G., Tayyar, Y., West, N., Zhang, P., McMillan, C.L.D., Soemardy, C., et al. (2021). A SARS-CoV-2 targeted siRNA-nanoparticle therapy for COVID-19. Mol. Ther. *29*, 2219–2226.

22. Gu, S.H., Yu, C.H., Song, Y., Kim, N.Y., Sim, E., Choi, J.Y., Song, D.H., Hur, G.H., Shin, Y.K., and Jeong, S.T. (2020). A Small interfering RNA lead targeting RNA-dependent RNA-polymerase effectively inhibit the SARS-CoV-2 infection in Golden Syrian hamster and Rhesus macaque. bioRxiv. https://doi.org/10.1101/2020.07.07.190967.

23. Chowdhury, U.F., Sharif Shohan, M.U., Hoque, K.I., Beg, M.A., Sharif Siam, M.K., and Moni, M.A. (2021). A computational approach to design potential siRNA molecules as a prospective tool for silencing nucleocapsid phosphoprotein and surface glycoprotein gene of SARS-CoV-2. Genomics *113*, 331–343.

24. Medeiros, I.G., Khayat, A.S., Stransky, B., dos Santos, S.E.B., de Assumpção, P.P., and de Souza, J.E.S. (2021). A small interfering RNA (siRNA) database for SARS-CoV-2 (2021). Sci. Rep. *11*, 8849.

25. Shawan, M., Sharma, A.R., Bhattacharya, M., Mallik, B., Akhter, F., Shakil, M.S., Hossain, M.M., Banik, S., Lee, S.S., Hasan, M.A., et al. (2021). Designing an effective therapeutic siRNA to silence RdRp gene of SARS-CoV-2. Infect. Genet. Evol. *93*, 104951.

26. Wu, R., and Luo, K.Q. (2021). Developing effective siRNAs to reduce the expression of key viral genes of COVID-19. Int. J. Biol. Sci. *17*, 1521–1529.

27. Blanchard, E.L., Vanover, D., Bawage, S.S., Tiwari, P.M., Rotolo, L., Beyersdorf, J., Peck, H.E., Bruno, N.C., Hincapie, R., Michel, F., et al. (2021). Treatment of influenza and SARS-CoV-2 infections via mRNA-encoded Cas13a in rodents. Nat. Biotechnol. *39*, 717–726.

28. Fareh, M., Zhao, W., Hu, W., Casan, J.M.L., Kumar, A., Symons, J., Zerbato, J.M., Fong, D., Voskoboinik, I., Ekert, P.G., et al. (2021). Reprogrammed CRISPR-Cas13b suppresses SARS-CoV-2 replication and circumvents its mutational escape through mismatch tolerance. Nat. Commun. *12*, 4270.

29. Abbott, T.R., Dhamdhere, G., Liu, Y., Lin, X., Goudy, L., Zeng, L., Chemparathy, A., Chmura, S., Heaton, N.S., Debs, R., et al. (2020). Development of CRISPR as an antiviral strategy to combat SARS-CoV-2 and influenza. Cell *181*, 865–876.e12.

30. Borel, F., Kay, M.A., and Mueller, C. (2014). Recombinant AAV as a platform for translating the therapeutic potential of RNA interference. Mol. Ther. *22*, 692–701.

31. Wang, D., Tai, P.W.L., and Gao, G. (2019). Adeno-associated virus vector as a platform for gene therapy delivery. Nat. Rev. Drug Discov. *18*, 358–378.

32. McCarty, D.M., Monahan, P.E., and Samulski, R.J. (2001). Self-complementary recombinant adeno-associated virus (scAAV) vectors promote efficient transduction independently of DNA synthesis. Gene Ther. *8*, 1248–1254.

33. Mendell, J.R., Al-Zaidy, S.A., Rodino-Klapac, L.R., Goodspeed, K., Gray, S.J., Kay, C.N., Boye, S.L., Boye, S.E., George, L.A., Salabarria, S., et al. (2021). Current clinical applications of gene therapy with AAVs. Mol. Ther. *29*, 464–488.

34. Hoffmann, M., Kleine-Weber, H., Schroeder, S., Krüger, N., Herrler, T., Erichsen, S., Schiergens, T.S., Herrler, G., Wu, N.-H., Nitsche, A., et al. (2020). SARS-CoV-2 cell entry depends on ACE2 and TMPRSS2 and is blocked by a clinically proven protease inhibitor. Cell *181*, 271–280.e8.

35. Wurtz, N., Penant, G., Jardot, P., Duclos, N., and La Scola, B. (2021). Culture of SARS-CoV-2 in a panel of laboratory cell lines, permissivity, and differences in growth profile. Eur. J. Clin. Microbiol. Infect. Dis. *40*, 477–484.

36. Lisowski, L., Dane, A.P., Chu, K., Zhang, Y., Cunningham, S.C., Wilson, E.M., Nygaard, S., Grompe, M., Alexander, I.E., and Kay, M.A. (2014). Selection and evaluation of clinically relevant AAV variants in a xenograft liver model. Nature *506*, 382–386.

37. Ai, J., Ibraheim, R., Tai, P.W.L., and Gao, G. (2017). A scalable and accurate method for quantifying vector genomes of recombinant adeno-associated viruses in crude lysate. Hum. Gene Ther. Methods *28*, 139–147.

38. Borner, K., Kienle, E., Huang, L.Y., Weinmann, J., Sacher, A., Bayer, P., Stullein, C., Fakhiri, J., Zimmermann, L., Westhaus, A., et al. (2020). Pre-arrayed pan-AAV peptide display libraries for rapid single-round screening. Mol. Ther. *28*, 1016–1032.

39. Grimm, D., and Kay, M.A. (2007). Combinatorial RNAi: a winning strategy for the race against evolving targets? Mol. Ther. *15*, 878–888.

40. Suhy, D.A., Kao, S.-C., Mao, T., Whiteley, L., Denise, H., Souberbielle, B., Burdick, A.D., Hayes, K., Wright, J.F., Lavender, H., et al. (2012). Safe, long-term hepatic expression of anti-HCV shRNA in a nonhuman primate model. Mol. Ther. *20*, 1737–1749.

41. Shah, P.S., Pham, N.P., and Schaffer, D.V. (2012). HIV develops indirect cross-resistance to combinatorial RNAi targeting two distinct and spatially distant sites. Mol. Ther. *20*, 840–848.

42. Herrera-Carrillo, E., and Berkhout, B. (2015). The impact of HIV-1 genetic diversity on the efficacy of a combinatorial RNAi-based gene therapy. Gene Ther. *22*, 485–495.

43. Amoasii, L., Long, C., Li, H., Mireault, A.A., Shelton, J.M., Sanchez-Ortiz, E., McAnally, J.R., Bhattacharyya, S., Schmidt, F., Grimm, D., et al. (2017). Single-cut genome editing restores dystrophin expression in a new mouse model of muscular dystrophy. Sci. Transl. Med. *9*, eaan8081.

44. Xie, J., Mao, Q., Tai, P.W.L., He, R., Ai, J., Su, Q., Zhu, Y., Ma, H., Li, J., Gong, S., et al. (2017). Short DNA hairpins compromise recombinant adeno-associated virus genome homogeneity. Mol. Ther. *25*, 1363–1374.

45. Wang, W., Xu, Y., Gao, R., Lu, R., Han, K., Wu, G., and Tan, W. (2020). Detection of SARS-CoV-2 in different types of clinical specimens. JAMA *323*, 1843–1844.

46. Xiao, F., Tang, M., Zheng, X., Liu, Y., Li, X., and Shan, H. (2020). Evidence for gastrointestinal infection of SARS-CoV-2. Gastroenterology *158*, 1831–1833.e3.

47. Stanifer, M.L., Kee, C., Cortese, M., Zumaran, C.M., Triana, S., Mukenhirn, M., Kraeusslich, H.G., Alexandrov, T., Bartenschlager, R., and Boulant, S. (2020). Critical role of type III interferon in controlling SARS-CoV-2 infection in human intestinal epithelial cells. Cell Rep. *32*, 107863.

48. Kumari, P., Rothan, H.A., Natekar, J.P., Stone, S., Pathak, H., Strate, P.G., Arora, K., Brinton, M.A., and Kumar, M. (2021). Neuroinvasion and encephalitis following intranasal inoculation of SARS-CoV-2 in K18-hACE2 mice. Viruses *13*, 132.

49. Leist, S.R., Dinnon, K.H., 3rd, Schäfer, A., Tse, L.V., Okuda, K., Hou, Y.J., West, A., Edwards, C.E., Sanders, W., Fritch, E.J., et al. (2020). A mouse-adapted SARS-CoV-2 induces acute lung injury and mortality in standard laboratory mice. Cell *183*, 1070–1085.e12.

50. Boden, D., Pusch, O., Lee, F., Tucker, L., and Ramratnam, B. (2003). Human immunodeficiency virus type 1 escape from RNA interference. J. Virol. *77*, 11531–11535.

51. Gitlin, L., Stone, J.K., and Andino, R. (2005). Poliovirus escape from RNA interference: short interfering RNA-target recognition and implications for therapeutic approaches. J. Virol. *79*, 1027.

52. ter Brake, O., Konstantinova, P., Ceylan, M., and Berkhout, B. (2006). Silencing of HIV-1 with RNA interference: a multiple shRNA approach. Mol. Ther. *14*, 883–892.

53. Baum, A., Fulton, B.O., Wloga, E., Copin, R., Pascal, K.E., Russo, V., Giordano, S., Lanza, K., Negron, N., Ni, M., et al. (2020). Antibody cocktail to SARS-CoV-2 spike protein prevents rapid mutational escape seen with individual antibodies. Science *369*, 1014–1018.

54. Bell, C.L., Vandenberghe, L.H., Bell, P., Limberis, M.P., Gao, G.P., Van Vliet, K., Agbandje-McKenna, M., and Wilson, J.M. (2011). The AAV9 receptor and its modification to improve in vivo lung gene transfer in mice. J. Clin. Invest. *121*, 2427–2435.

55. Grimm, D., and Zolotukhin, S. (2015). E pluribus unum: 50 years of research, millions of viruses, and one goal–tailored acceleration of AAV evolution. Mol. Ther. *23*, 1819–1831.

56. Sims, J.J., Greig, J.A., Michalson, K.T., Lian, S., Martino, R.A., Meggersee, R., Turner, K.B., Nambiar, K., Dyer, C., Hinderer, C., et al. (2021). Intranasal gene therapy to prevent infection by SARS-CoV-2 variants. PLoS Pathog. *17*, e1009544.

57. Weinmann, J., Weis, S., Sippel, J., Tulalamba, W., Remes, A., El Andari, J., Herrmann, A.K., Pham, Q.H., Borowski, C., Hille, S., et al. (2020). Identification of a myotropic AAV by massively parallel in vivo evaluation of barcoded capsid variants. Nat. Commun. *11*, 5432.

58. Korbelin, J., Sieber, T., Michelfelder, S., Lunding, L., Spies, E., Hunger, A., Alawi, M., Rapti, K., Indenbirken, D., Muller, O.J., et al. (2016). Pulmonary targeting of adeno-associated viral vectors by next-generation sequencing-guided screening of random capsid displayed peptide libraries. Mol. Ther. *24*, 1050–1061.

59. Grimm, D., Streetz, K.L., Jopling, C.L., Storm, T.A., Pandey, K., Davis, C.R., Marion, P., Salazar, F., and Kay, M.A. (2006). Fatality in mice due to oversaturation of cellular microRNA/short hairpin RNA pathways. Nature *441*, 537–541.

60. Patel, K., Kilfoil, G., Wyles, D.L., Naggie, S., Lawitz, E., Bradley, S., Lindell, P., and Suhy, D. (2016). 258. Phase I/IIa study of TT-034, a DNA-directed RNA interference (ddRNAi) agent delivered as a single administration for the treatment of subjects with chronic hepatitis C virus (HCV). Mol. Ther. *24*, S102.

61. O'Donnell, J.S., and Chappell, K.J. (2021). Chronic SARS-CoV-2, a cause of post-acute COVID-19 sequelae (long-COVID)? Front. Microbiol. *12*, 724654.

62. Brown, L.K., Moran, E., Goodman, A., Baxendale, H., Bermingham, W., Buckland, M., AbdulKhaliq, I., Jarvis, H., Hunter, M., Karanam, S., et al. (2021). Treatment of chronic or relapsing COVID-19 in immunodeficiency. J. Allergy Clin. Immunol. https://doi.org/10.1016/j.jaci.2021.10.031.

63. Kemp, S.A., Collier, D.A., Datir, R.P., Ferreira, I., Gayed, S., Jahun, A., Hosmillo, M., Rees-Spear, C., Mlcochova, P., Lumb, I.U., et al. (2021). SARS-CoV-2 evolution during treatment of chronic infection. Nature *592*, 277–282.

64. Buckland, M.S., Galloway, J.B., Fhogartaigh, C.N., Meredith, L., Provine, N.M., Bloor, S., Ogbe, A., Zelek, W.M., Smielewska, A., Yakovleva, A., et al. (2020). Treatment of COVID-19 with remdesivir in the absence of humoral immunity: a case report. Nat. Commun. *11*, 6385.

65. Zincarelli, C., Soltys, S., Rengo, G., and Rabinowitz, J.E. (2008). Analysis of AAV serotypes 1-9 mediated gene expression and tropism in mice after systemic injection. Mol. Ther. *16*, 1073–1080.

66. Blenkinsopp, W.K. (1967). Proliferation of respiratory tract epithelium in the rat. Exp. Cell Res. *46*, 144–154.

67. Rawlins, E.L., and Hogan, B.L. (2008). Ciliated epithelial cell lifespan in the mouse trachea and lung. Am. J. Physiol. Lung Cell. Mol. Physiol. *295*, L231–L234.

68. Sender, R., and Milo, R. (2021). The distribution of cellular turnover in the human body. Nat. Med. *27*, 45–48.

69. Chan, K.Y., Jang, M.J., Yoo, B.B., Greenbaum, A., Ravi, N., Wu, W.L., Sanchez-Guardado, L., Lois, C., Mazmanian, S.K., Deverman, B.E., et al. (2017). Engineered AAVs for efficient noninvasive gene delivery to the central and peripheral nervous systems. Nat. Neurosci. *20*, 1172–1179.

70. Polyak, S., Mach, A., Porvasnik, S., Dixon, L., Conlon, T., Erger, K.E., Acosta, A., Wright, A.J., Campbell-Thompson, M., Zolotukhin, I., et al. (2012). Identification of adeno-associated viral vectors suitable for intestinal gene delivery and modulation of experimental colitis. Am. J. Physiol. Gastrointest. Liver Physiol. *302*, G296–G308.

71. Hou, Y.J., Okuda, K., Edwards, C.E., Martinez, D.R., Asakura, T., Dinnon, K.H., 3rd, Kato, T., Lee, R.E., Yount, B.L., Mascenik, T.M., et al. (2020). SARS-CoV-2 reverse genetics reveals a variable infection gradient in the respiratory tract. Cell *182*, 429–446.e14.

72. Mossel, E.C., Wang, J., Jeffers, S., Edeen, K.E., Wang, S., Cosgrove, G.P., Funk, C.J., Manzer, R., Miura, T.A., Pearson, L.D., et al. (2008). SARS-CoV replicates in primary human alveolar type II cell cultures but not in type I-like cells. Virology *372*, 127–135.

73. Cortese, M., Lee, J.Y., Cerikan, B., Neufeldt, C.J., Oorschot, V.M.J., Kohrer, S., Hennies, J., Schieber, N.L., Ronchi, P., Mizzon, G., et al. (2020). Integrative imaging reveals SARS-CoV-2-induced reshaping of subcellular morphologies. Cell Host Microbe *28*, 853–866.e5.

74. Fujii, M., Matano, M., Toshimitsu, K., Takano, A., Mikami, Y., Nishikori, S., Sugimoto, S., and Sato, T. (2018). Human intestinal organoids maintain self-renewal capacity and cellular diversity in niche-inspired culture condition. Cell Stem Cell *23*, 787–793.e6.

75. Matsushita, T., Elliger, S., Elliger, C., Podsakoff, G., Villarreal, L., Kurtzman, G.J., Iwaki, Y., and Colosi, P. (1998). Adeno-associated virus vectors can be efficiently produced without helper virus. Gene Ther. *5*, 938–945.

76. Grosse, S., Penaud-Budloo, M., Herrmann, A.-K., Börner, K., Fakhiri, J., Laketa, V., Krämer, C., Wiedtke, E., Gunkel, M., Ménard, L., et al. (2017). Relevance of assembly-activating protein for adeno-associated virus vector production and capsid protein stability in mammalian and insect cells. J. Virol. *91*, e01198–e01217.

77. Herrmann, A.-K., Bender, C., Kienle, E., Grosse, S., El Andari, J., Botta, J., Schürmann, N., Wiedtke, E., Niopek, D., and Grimm, D. (2019). A robust and all-inclusive pipeline for shuffling of adeno-associated viruses. ACS Synth. Biol. *8*, 194–206.

78. Klein, S., Cortese, M., Winter, S.L., Wachsmuth-Melm, M., Neufeldt, C.J., Cerikan, B., Stanifer, M.L., Boulant, S., Bartenschlager, R., and Chlanda, P. (2020). SARS-CoV-2 structure and replication characterized by in situ cryo-electron tomography. Nat. Commun. *11*, 5885.

79. Menachery, V.D., Gralinski, L.E., Baric, R.S., and Ferris, M.T. (2015). New metrics for evaluating viral respiratory pathogenesis. PLoS One *10*, e0131451.

80. Li, H., and Durbin, R. (2009). Fast and accurate short read alignment with Burrows-Wheeler transform. Bioinformatics *25*, 1754–1760.

81. Li, H., Handsaker, B., Wysoker, A., Fennell, T., Ruan, J., Homer, N., Marth, G., Abecasis, G., and Durbin, R. (2009). The sequence alignment/map format and SAMtools. Bioinformatics *25*, 2078–2079.

82. Cingolani, P., Platts, A., Wang le, L., Coon, M., Nguyen, T., Wang, L., Land, S.J., Lu, X., and Ruden, D.M. (2012). A program for annotating and predicting the effects of single nucleotide polymorphisms, SnpEff: SNPs in the genome of Drosophila melanogaster strain w1118; iso-2; iso-3. Fly *6*, 80–92.

83. R Core Team (2020). R: A Language and Environment for Statistical Computing (R Foundation for Statistical Computing).